NASA TECHNICAL NOTE

NASA TN D-3312

NASA TN D-3312

A STUDY OF THE PRESSURE, HEAT TRANSFER, AND SKIN FRICTION ON SHARP AND BLUNT FLAT PLATES AT MACH 6.8

by Luther Neal, Jr.

Langley Research Center
Langley Station, Hampton, Va.

NATIONAL AERONAUTICS AND SPACE ADMINISTRATION • WASHINGTON, D. C. • APRIL 1966

NASA TN D-3312

A STUDY OF THE PRESSURE, HEAT TRANSFER, AND SKIN FRICTION

ON SHARP AND BLUNT FLAT PLATES AT MACH 6.8

By Luther Neal, Jr.

Langley Research Center
Langley Station, Hampton, Va.

NATIONAL AERONAUTICS AND SPACE ADMINISTRATION

A STUDY OF THE PRESSURE, HEAT TRANSFER, AND SKIN FRICTION
ON SHARP AND BLUNT FLAT PLATES AT MACH 6.8[*]

By Luther Neal, Jr.
Langley Research Center

SUMMARY

A study of the pressure, heat-transfer, and skin-friction distributions over a flat plate with both sharp and blunt leading edges has been conducted at a nominal free-stream Mach number of 6.8, over a range of free-stream Reynolds number per centimeter from about 0.02×10^6 to 0.16×10^6, and at a wall-to-stagnation temperature ratio of about 0.5. The model consisted of a 25.4-cm-wide by 61-cm-long flat plate equipped with interchangeable leading edges having thicknesses of 0.0025, 0.25, and 1.27 cm. The investigation covered all three flow regimes — laminar, transitional, and turbulent.

The results showed no significant effect on the pressure distribution of a sixfold change in Reynolds number for the 1.27-cm-thick leading edge for surface distances up to about 20 times the leading-edge thickness. However, for the 0.25-cm-thick leading edge, viscous effects were obtained which were roughly of the same order of magnitude as those found for the "sharp" (0.0025 cm thick) leading edge. The agreement between theoretical and experimental pressures could generally be classified as fair to good for the particular theories employed.

Comparison of the laminar and turbulent skin-friction and heat-transfer data with corresponding theoretical estimates showed both agreement and disagreement, depending, among other things, upon the leading-edge thickness, the particular theory used, and for the turbulent data, the position used for the virtual origin. Small and moderate leading-edge blunting delayed transition whereas the largest blunting produced about the same transition Reynolds number as the sharp leading edge. Also, for the sharp leading edge, good agreement between measured skin-friction and heat-transfer results was obtained, for both laminar and turbulent flow, with use of particular forms of the Reynolds analogy. For the blunt leading edges, however, no conclusion regarding the Reynolds analogy

concept could be made because of the unknown magnitude of the skin-friction balance gap effects. These effects were almost certain to be present because of the existence of a sizable pressure gradient associated with the blunt leading edges.

INTRODUCTION

At hypersonic speeds there are two outstanding features which characterize continuum flow around a thin body. One is the displacement effect of the boundary layer and the other is the effect due to leading-edge bluntness. At these speeds the boundary layers are much thicker than those at lower Mach numbers because of the large temperature gradients across the boundary layer. Therefore, the body shape in effect tends to be significantly distorted by these thick boundary layers. The amount of the distortion is represented by the boundary-layer displacement thickness which, for large Mach numbers and hot surfaces, approaches the total thickness of the boundary layer. As a consequence of this effective body distortion, the local pressures over the body are altered from the inviscid values.

When the leading edge is blunted, the flow field is further complicated. The blunt-leading-edge shock causes high pressures to persist on the body surface downstream of the leading edge, and these induced pressures decay with downstream distance. This behavior of the pressure distribution is usually referred to as the blast-wave effect.

In the earlier theoretical work on induced pressure effects, the boundary-layer displacement effects and the leading-edge-bluntness effects were treated separately, except for the early and crude treatment of the combined problem in reference 1. References 1 to 5 consider both the weak and strong interaction regimes associated with pure viscous effects. In the weak interaction regime, the induced pressures due to boundary-layer displacement effects are not large enough to have an important effect on the boundary-layer growth. Conversely, in the strong interaction regime, large viscid-induced pressures occur which do have an important effect on the boundary-layer growth. In this region, the mutual interaction between the boundary layer and the boundary-layer-induced pressure must be considered. The theory of reference 5 actually makes no distinction between strong and weak interaction and thus gives a continuous variation between the two regimes. At the other end of the spectrum, leading-edge bluntness effects have been treated in references 6 to 9. Because of the complexity of the problem, rigorous treatment of the two effects simultaneously has proceeded at a slower pace. References 10 to 12, however, have dealt with this problem in considerable detail.

A problem area closely connected with these induced pressures is their corresponding effects on the skin friction and heat transfer. Not only is the pressure level important here but also the pressure gradient. Also, when the leading edge is blunted,

most of the fluid particles near the surface have passed through the strong portion of the leading-edge shock. This results in the appearance of a high-entropy layer close to the surface which can swallow the boundary layer. These types of problems are considered in references 12 to 15.

Results from experimental investigations of similar scopes have been published concurrently with the previously mentioned theoretical work. A large portion of the experimental work is included in references previously cited. The theoretical and experimental results have tended to support each other. There are, nevertheless, fruitful areas remaining to be investigated. For example, the region far downstream from a blunt leading edge needs some attention. One extremely useful method for predicting the induced effects due to leading-edge bluntness, for both two- and three-dimensional bodies, has evolved from the blast-wave theory. However, this method is not expected to apply either close to the nose where the shock is too strong or far downstream where the shock is too weak (ref. 9). Exactly how far downstream useful results can be obtained has not been well established. In addition, natural transition on both sharp and blunt plates needs further study. Evaluation of the relation between skin friction and heat transfer is another problem, especially where there is a large pressure gradient. There are also other worthwhile pursuits such as comprehensive studies of wall temperature effects.

The purpose of the present investigation was to study some of the foregoing problem areas. In the investigation, which was conducted at a Mach number of 6.8, pressure, heat-transfer, and skin-friction distributions over a flat plate with various degrees of leading-edge blunting were obtained. The scope of the investigation permitted bluntness effects, Reynolds number effects, and the relation between skin friction and heat transfer to be studied. All three boundary-layer flow regimes — laminar, transitional, and turbulent — were encountered.

SYMBOLS

C_f	local skin-friction coefficient
N_{St}	local Stanton number
c_m	specific heat of model
c_p	specific heat of air at constant pressure
h_w	local heat-transfer coefficient at wall
K_1, K_3	correction functions in the laminar-skin-friction and heat-transfer equations, respectively, due to pressure gradient apart from pressure level, defined in reference 13

M	Mach number
n	exponent defined by $p_w \propto x^n$
p	pressure
N_{Pr}	Prandtl number
$\dot{q}$	local heating rate to model per unit area
q_∞	free-stream dynamic pressure
R	Reynolds number per centimeter
$R_{\infty,x}$	free-stream Reynolds number based on distance from leading edge
$R_{\infty,\Delta x}$	free-stream effective Reynolds number for the turbulent data (see sketch, page 16)
$(R_{\infty,t})_{tr}$	transitional Reynolds number based on leading-edge thickness and free-stream conditions
S	flat surface area of skin-friction patch
t	model-leading-edge thickness (fig. 4)
t_s	local skin thickness of heat-transfer panel
T	absolute temperature
U_∞	free-stream velocity
x,x',y,z	model coordinates (fig. 4)
X,Y,Z	nozzle coordinates (fig. 4)
δ^*	boundary-layer displacement thickness
ρ_m	density of model
ρ_∞	free-stream density of air
τ	time measured from start of tunnel run

Subscripts:

aw	adiabatic wall

i	inviscid
w	wall
l	local (at edge of boundary layer)
∞	free stream
t	conditions in stagnation chamber

Abbreviations:

H.T.	heat transfer
S.F.B.	skin-friction balance
w	with
w/o	without
V.O.	virtual origin

APPARATUS AND TESTS

Tunnel and Nozzle

The tests were conducted in the Langley 11-inch hypersonic tunnel which is shown schematically in figure 1 and described in reference 16. The nozzle used during the tests was two dimensional with contours constructed of invar and provided a nominal free-stream Mach number of about 6.8. The test-section Mach number of this nozzle varies slightly with both unit Reynolds number (or stagnation pressure for a given value of stagnation temperature) and time. The variation with unit Reynolds number results mainly from changes in the nozzle-wall boundary-layer thickness whereas the variation with time results from slight distortion of the throat section due to thermal expansion. The Mach number variation with time, however, is considerably less for this invar nozzle than it was for an earlier Mach 6.8 steel nozzle described in reference 17.

Figure 2 shows excerpts from a 1961 calibration of the invar nozzle, which illustrates the Mach number variation previously noted. For a 60-sec run $\left(\text{constant } p_t \text{ and } T_t\right)$ the Mach number varies about 0.05. Changing the stagnation pressure from 5 to 40 atm $\left(T_t \approx 610^{\circ} \text{ K}\right)$ results in a change in free-stream Mach number from about 6.7 to 6.9. Also shown in figure 2 are results from a check calibration in support of the present investigation. Results obtained on the test-section longitudinal center line (X = 0) and also 28 cm ahead of the center line are given. This latter location corresponds to the approximate longitudinal position of the leading edge for the present model

5

mounting. The present results for both locations agree well with the previous calibration. Both calibrations were obtained by numerically averaging the Mach number for various points in the usable core. Typical vertical and horizontal Mach number distributions are shown in figure 3, which illustrates the magnitude of variation present at a given cross section and also the size of the usable core. As these local Mach numbers were calculated from pitot pressure measurements by assuming an isentropic expansion from the stagnation conditions, the indicated Mach numbers in the tunnel boundary layer are in error.

In the present investigation, the instrumented side of the flat-plate model practically coincided with the vertical center line of the nozzle. Most of the data presented are for the center-line ray of the model. Also, the maximum leading-edge thickness is small compared with the usable core size. Consequently, the center line or near-center-line Mach number is more representative for analysis of the data than the average core Mach number typified in figure 2. Therefore, for data reduction purposes, the average Mach number in a 2.5-cm-square cross section was used. The cross section chosen was the one corresponding to the approximate location of the leading edge of the model $(X \approx -28 \text{ cm})$. For this station, the average Mach number in this reduced cross section was about 1 percent lower than the average core Mach number; whereas, for $X = 0$, it was approximately the same as the average core Mach number.

Model

A sketch of the model and model support system is given in figure 4. The model was constructed of 347 stainless steel and consisted of a 25.4-cm by 61-cm flat plate with interchangeable noses of various leading-edge thickness. The 0.0025- and 0.25-cm-thick leading edges had 20° bevels on the top side. The 1.27-cm-thick leading edge was formed by adding a wedge which covered the bevelled portion of the 0.25-cm-thick leading edge. Rearward of $x' = 12.07$ cm, a center strip 10.80 cm wide was removable to facilitate mounting of various instrumented panels. Individual drawings of these various panels are given in figure 5. The skin-friction panel could be located at 2.54-cm intervals between $x' = 14.60$ cm and $x' = 52.70$ cm. Filler panels were used to fill the remaining space. One filler panel used during most of the skin-friction tests was equipped with a dummy skin-friction patch (gap sealed). The dummy patch was instrumented with five thermocouples which provided check information on the surface temperature. The pressure and heat-transfer inserts were identical except for the slots which were milled in the back side of the heat-transfer panel in order to obtain a thinner skin. The pressure orifices were formed from tubing of 0.15-cm inside diameter, which also made up the remaining pressure ducting system. The thermocouples were spotwelded to the back side of the heat-transfer panel. Both the pressure tubing and thermocouple

leads were routed through the rear of the model support and then through either the top or side of the tunnel wall to the appropriate recording instruments.

The various inserts were tongue-grooved in the spanwise direction and were held in place by small counter-sunk screws placed along each side of the inserts. The screw heads were covered over with dental plaster so as to form a "smooth" surface. In spite of the extreme care taken while changing inserts or working in general with the model, an occasional scratch would occur. When one did develop, however, it was carefully finished down by hand methods.

Measurements of the model with the skin-friction filler panels in place showed that the maximum deviation from a "flat" surface was about ± 0.001 cm per cm; the total deviation over the complete 61-cm length was about ± 0.008 cm. Similar measurements with the pressure and heat-transfer panel inserts in place indicated deviations roughly double those of the skin-friction model. Profilometer rms readings over the model showed that the surface finish, excluding a few scratches, the seams between the various removable inserts, and the plastered-over screw heads associated with the removable pieces, was less than 25×10^{-6} cm.

As shown in figure 4, the model nearly spanned the complete width of the tunnel. Hence, much of the uninstrumented portion of the model extended into the tunnel boundary layer. The primary reason for selecting the model wider than the uniform core was the desiring of as long a chordwise run as feasible uninfluenced by disturbances from the sides or leading-edge tips. It will be recalled that Coles in his now-classical skin-friction work of reference 18 also employed a model that protruded into the tunnel boundary layer; in fact, his model completely spanned the tunnel. Other investigators have used similar models (refs. 19 and 20). In permitting any model to extend into the tunnel boundary layer, there is a possibility of obtaining other disturbances. In view of this possibility, surface oil-flow studies were conducted in the present investigation. The results of these studies will be subsequently discussed.

In order to reduce flow around the sides of the model, side plates were employed; sketches of the two sets used are shown in figure 6. Both sets were constructed of 416 steel and were ground sharp at the edges. The set shown in figure 6(a) had the front ends shaped approximately to the center-line shock for the sharp-leading-edge model and was used exclusively for tests involving this leading edge. The set shown in figure 6(b) had the front ends shaped approximately to the center-line shock of the 1.27-cm-thick leading-edge model, but was used for both blunt leading edges investigated. Since the model protruded into the tunnel boundary layer, it is recognized that the shapes of the side plates may not have been optimum. However, surface oil-flow studies did indicate beneficial effects from the side plates.

Instrumentation

The stagnation pressure was read from a Bourdon tube gage and the stagnation temperature was obtained by using chromel-alumel thermocouples. The surface pressures were measured on aneroid-type six-cell recording units described in reference 16. These units convert the deflection of a diaphragm into a rotation of a small mirror, which in turn reflects a beam of light onto a moving film; thus, a time history of the measured pressure is recorded. The outputs of the chromel-alumel model thermocouples were recorded on oscillographs, which similarly provided a time history of the surface temperature of the model.

The local skin friction was measured with a highly sensitive skin-friction balance, which is shown schematically in figure 7. The skin-friction patch (2.54 cm in diameter) was supported by four cantilever beams that were stiff in the center but extremely thin and flexible at each end. A dampening rod (not shown), which was coated with oil, extended through the patch parallel with the flow. As the patch deflected under load, the movement was sensed by a differential transformer arrangement which activated a nullifying device which returned the patch to the null position. Thus, the clearance (0.0025 cm) between the patch and the model remained constant during all gathering of the data. Figure 8 shows the results of a typical calibration as well as the calibration setup. The output of the skin-friction balance was recorded on a self-balancing potentiometer with a range of 0 to 10 millivolts or 0 to 50 millivolts, depending upon the level of output.

The balance chamber was sealed except for the gap around the patch and two pressure bleeds which were installed approximately 1 cm from the sides of the patch and 0.46 cm rearward (see fig. 5(c)) for the purpose of quickly equalizing the pressure between the surface and the chamber at the start of the run. Except for a few cases the pressure in the balance chamber was monitored during the runs for later comparison with measured surface pressures. The chamber pressure generally agreed well with the average surface pressure over the same region.

The degree of flushness of the skin-friction patch relative to the adjacent surface cannot be quoted for most of the skin-friction data for the sharp leading edge, as the balance was damaged before this measurement was recorded; however, at initial assembly, the patch and adjacent surface were lapped in order to insure "flushness." After the damaged balance had been repaired, additional sharp-leading-edge data as well as all of the blunt-leading-edge data were obtained. For this later series of tests, measurements indicated that the patch, which was not lapped at reassembly, was protruded approximately 0.0005 cm. Results from these additional sharp-leading-edge tests (including some repeat runs) showed no systematic deviation from the previous data.

From the results of reference 21, a patch misalinement of 0.0005 cm would be expected to produce a nominal error of 1 percent or less.

Test Conditions and Procedures

The tests were conducted at stagnation pressures ranging from 5 to 40 atm, which corresponded to a free-stream Mach number, based on a 2.5-cm cross section at $X = -28$ cm, from about 6.6 to 6.8. The average stagnation temperature was around 615° K, which was sufficient to prevent liquefaction of the air in the test section. The corresponding free-stream Reynolds number per centimeter ranged from about 0.02×10^6 to 0.16×10^6. Water condensation effects were eliminated by keeping the absolute humidity of the air sufficiently low.

Nominal values for the wall temperature functions are as follows:

$$\frac{T_w}{T_t} \approx 0.5 \quad \text{(sharp and blunt)}$$

$$\frac{T_w}{T_\infty} \approx \frac{T_w}{T_l} \approx 5.2 \quad \text{(sharp)}$$

$$\frac{T_w}{T_l} \approx 1.3 \text{ to } 1.6 \quad \text{(blunt or normal shock loss)}$$

All tests, however, were carried out under varying model surface temperatures which was, of course, due to aerodynamic heating to the model as the run time progressed. The amount of temperature rise observed for the short-duration heat-transfer runs was only a few degrees. No detailed temperature measurements were made simultaneously with the skin-friction or pressure measurements, but for most of the skin-friction tests, surface-temperature information was recorded at various given locations on the model as a function of time. Samples of these data are presented in figure 9. The greater increases in temperature at the higher unit Reynolds numbers are a result of the increased heat transfer due to the transitional and turbulent flow.

DATA REDUCTION

The local heating rate was computed from the following thin-skin equation

$$\dot{q}_w = c_m \rho_m t_s \frac{dT_w}{d\tau}$$

where the rate of surface-temperature rise was obtained from the oscillograph records at a time near the start of a test run. This time was of the order of 1 to 2 sec, which was the amount required, using the quick-starting technique, for conditions of pressure and

9

temperature to stabilize in the settling chamber. This quick-starting technique is an approximation to an applied step function in the heat-transfer coefficient. The density and specific heat of the 347 stainless steel were taken to be 7.81 g/cm^3 $\left(0.282\ lb_m/in^3\right)$ and 0.142 J/g-^{O}K $\left(0.11\ Btu/lb_m-^OR\right)$, respectively.

The local heat-transfer coefficient was calculated from the relation

$$h_w = \frac{\dot{q}_w}{T_{aw} - T_w}$$

in which conduction corrections were found to be negligible. Although the measured surface temperature was used here, its deviation from about 305° K was generally less than 6°. The adiabatic-wall temperature was obtained from figure 10 using the experimental pressure data. The values of T_{aw}/T_t given in this figure were calculated by assuming the recovery factor to be equal to the square root and cube root of the Prandtl number for laminar and turbulent flow, respectively. The appropriate Prandtl numbers were evaluated at temperatures corresponding to Monaghan's T-prime temperature for insulated plates (refs. 22 and 23). The values of Prandtl number as a function of temperature were taken as those given in reference 24. The curves designated "sharp" correspond to assuming a local total pressure equal to that behind an oblique shock whose strength will produce the local pressure ratio whereas those designated "blunt" correspond to assuming a local total pressure equal to the stagnation pressure behind a normal shock. For the transitional data, a linear variation between the laminar and turbulent adiabatic-wall temperatures was used, as was used in reference 25; however, the typical appearance of a plot of h_w against x in the transition region indicates that a sinusoidal variation would perhaps have been more appropriate. Unless otherwise specified, the heat-transfer data presented for the 0.25- and 1.27-cm-thick leading edges were reduced by using the "blunt" curves of figure 10.

The Stanton number, based on free-stream conditions, was computed from its definition

$$N_{St,\infty} = \frac{h_w}{c_p \rho_\infty U_\infty}$$

The local skin-friction coefficient was computed from the equation

$$C_{f,\infty} = \frac{F_{total}}{q_\infty S}$$

where S is the flat surface area of the disk and F_{total} is the total force sensed by the disk of the skin-friction element. No correction was made for any buoyance force, because detail pressure distributions necessary for obtaining such forces were not

obtained. Further discussion concerning this matter is delayed until the skin-friction data are presented.

In reducing all the experimental data, account was taken of the previously noted slight variation of free-stream Mach number with both time and stagnation pressure. No attempt has been made to "adjust" the data to correspond to a constant Mach number.

RESULTS AND DISCUSSION

Flow Visualization

Surface oil-flow studies.- In order to determine the nature of the shear direction over the model, surface oil-flow studies were made. This was accomplished by placing small dots or spanwise strips of a mixture of oil and lampblack on the surface, and then exposing the model to the flow. A postrun photograph of the sharp-leading-edge dummy model, without side plates, is shown in figure 11(a) for $R_\infty \approx 0.15 \times 10^6$. The combined effect of edge proximity and tunnel boundary layer on shear direction is quite apparent. It should be pointed out that these oil streaks represent the direction of shear within the inner edge of the boundary layer and do not necessarily reflect the flow direction at the outer edge of the model boundary layer. However, for uniform near-parallel streaks it can reasonably well be assumed that the flow is, for all practical purposes, two dimensional. Roughly, then, the center one-half strip of the model span is subjected to uniform flow over the forward part of the model. However, the width of the uniform region decreases quite drastically toward the rear of the model. Adding side plates (fig. 11(b)) provides a noted improvement on the rearward part of the model. There appears to be some additional waviness to the traces on the forward portion of the model due to adding the side plates; however, this condition did not consistently occur at other Reynolds numbers.

Figure 12 shows samples of postrun oil-flow photographs taken of the model with blunt leading edges (and with side plates). These photographs show that the blunt-leading-edge data for the rearward portion of the model should be discarded because of the well-defined interference effects noted there. These interference effects appear to originate at the two outer tip regions of the leading edge and are swept rearward until they eventually meet each other on the rearward portion of the model. Because of the complex nature of the flow near the leading-edge tips, the exact cause of these interference effects cannot easily be pinpointed. For example, there is a model boundary layer developing in a turbulent tunnel-wall boundary layer and being further complicated by the horizontal component of the strong bow shock being thrown toward and reflected away from the side wall.

<u>Schlieren photographs</u>.- Schlieren photographs of the model, without side plates, are shown in figure 13 for a constant unit Reynolds number. Two photographs for each leading edge are shown — one with the model in the standard position of $X \approx -28$ cm and the other with it moved rearward 12 cm which permitted the nose region to be photographed. These photographs have several undue markings resulting from film scarring by a defective roller.

For the sharp leading edge, the boundary layer is readily discernible and its influence upon the initial curvature of the leading-edge shock can likewise be noted. As the leading edge is blunted, the boundary layer becomes less discernible and for $t = 1.27$ cm, it cannot be seen because of the overriding influence of the shear layer produced by the blunt nose. Of particular interest, insofar as the shock structure for the blunt leading edges is concerned, is the secondary nose shock. This shock apparently results from the recompression that normally follows the overexpansion around a square-shape leading edge.

Spanwise Variations and Qualitative Effects of Side Plates

In figure 14, pressure and heat-transfer data are presented for $y = 0$ and $y = 1.9$ cm at two unit Reynolds numbers to illustrate the amount of spanwise variation present. Also, data are shown with and without side plates to illustrate their effects. Insofar as sizable spanwise variations are concerned, the only systematic ones noted were in the heat-transfer data on the forward part of the sharp-leading-edge model where the center-line values generally were from about 5 to 10 percent higher than those at $y = 1.9$ cm. It may be worthwhile to note that a 1-percent uncertainty in local stagnation temperature results in approximately a 2-percent uncertainty in the parameter $N_{St,\infty} \sqrt{R_{\infty,x}}$ for the present test conditions.

The effects of side plates can be noted by comparing the flagged and unflagged data symbols. For the sharp leading edge no appreciable effects are noted up to $x \approx 40$ cm, although there appears to be a tendency for the values without side plates to be slightly lower. Rearward of this location, however, the pressure and heat-transfer parameters are somewhat decreased by adding side plates. This decrease in the heat-transfer parameter is due in part to slightly later boundary-layer transition. For the blunt leading edges, the pressure tends to be slightly lower without side plates than it is with them, whereas the reverse appears to be true for the heat-transfer parameter. Similar results for a blunt cylindrical leading edge were observed in reference 26. No data are presented for the blunt leading edges beyond the midpoint of the plate because of the interference effects in this region as previously discussed.

Side plates can perturb the flow as mentioned in reference 26 and shown in figure 11, but they are believed to be more beneficial than detrimental insofar as the

present investigation is concerned. Hence, the data presented in the remainder of the paper will be for the case with side plates.

Nature of Leading-Edge-Bluntness Effects

Before presenting the experimental effects of leading-edge bluntness on the skin-friction, heat-transfer, and pressure distributions, it is of interest to look first at some calculated values of local flow and boundary-layer characteristics in order to obtain general orientation. For conditions close to those of the present investigation, the ratios of various blunt-leading-edge parameters to similar sharp-leading-edge parameters are shown in figure 15 as a function of x/t. (For a given value of x/t, the value of x for the sharp leading edge is the same as that for the blunt leading edge.) In these calculations, the displacement effect of the boundary layer has been neglected in evaluating the local flow properties. Thus, for the sharp leading edge $p_l = p_\infty$ for all values of x and for the blunt leading edges $p_l = p_{l,i}$. Also, for the blunt leading edge, the boundary layer is assumed to be submerged within the high-entropy layer associated with the near normal portion of the leading-edge shock. The local Reynolds number is affected most by this later assumption, being reduced by about 90 percent. Also, the local Mach number is reduced considerably. The local heat-transfer coefficient can either be increased or decreased depending upon the pressure level. However, there would be little deviation of the heat-transfer-coefficient ratio at any value of x/t from the asymptotic value of 0.92 (where $p/p_\infty = 1$) if it was divided by the square root of the pressure ratio. Similarly, the boundary-layer-displacement thickness ratio would deviate little from its asymptotic value of 0.93 if it was multiplied by the square root of the pressure ratio. (The boundary-layer characteristics shown are based upon Monaghan's T-prime method (ref. 22).)

Figure 16 shows a comparison of the predicted and measured effects of leading-edge blunting on the pressure, heat-transfer, and skin-friction parameters for various unit Reynolds numbers. The effect of leading-edge blunting on the pressure distribution (fig. 16(a)) is quite pronounced, especially for the thicker leading edge. The bluntness-effect trend, however, is predicted satisfactorily by the method of reference 9.

For the lower unit Reynolds number, the effect of nose blunting on the heat-transfer parameter is fairly sizable (fig. 16(b)). The experimental data for $t = 0.25$ cm are approximately 25 percent lower than those for $t = 0.0025$ cm, whereas T-prime theory predicts little difference between the two cases. One primary cause of the failure of theory to predict this difference probably is the neglect of the pressure-gradient effect. According to reference 13, this effect would reduce the theoretical estimates by approximately 14 percent for the conditions where $p_w \propto x^{-0.33}$, which approximates the experimental pressure data for $t = 0.25$ cm. Thus, if the pressure-gradient effect was taken

into account, the bluntness-effect trend would be predicted, but then poorer agreement would result between the theoretical estimates and the experimental data for the blunt leading edges. This latter result would be somewhat similar to that which already exists for the sharp leading edge, as the data are about 20 percent higher than theory. However, as illustrated in figure 17, the ratio of blunt-leading-edge values of $N_{St,\infty}\sqrt{R_{\infty,x}}$ to sharp-leading-edge values is predicted fairly satisfactorily if the pressure-gradient effect is taken into account.

At the higher unit Reynolds number (see fig. 16(b)), where transition is occurring for the sharp leading edge, moderate blunting delays transition whereas the reverse is true for large blunting. This same effect at the higher unit Reynolds number is seen in the skin-friction data presented in figure 16(c). Also, for the laminar data, the bluntness-effect trend is predicted fairly satisfactorily, although the actual magnitude ranges from about 20 to 50 percent higher than theory. If the ratio of blunt-leading-edge values of $C_{f,\infty}\sqrt{R_{\infty,x}}$ to sharp-leading-edge values is considered, then the agreement between experiment and the zero-pressure-gradient theory is better. Part of the discrepancies between theory and experiment for the blunt leading edge is due to the "gap effect," which, unfortunately, was not determined in the present investigation. Further discussion of this matter is given in the next section of this paper. It might be mentioned that the laminar skin-friction pressure-gradient parameter K_1 of reference 13 is approximately unity, even for large negative pressure gradients under the present conditions.

As mentioned previously, the boundary layer was assumed to be submerged in the high-entropy layer at all times unless specifically designated otherwise for the two blunt leading edges. Whether or not this assumption is valid is not extremely important from the laminar heat-transfer standpoint as shown in figure 18 where values of $N_{St,\infty}\sqrt{R_{\infty,x}}$ are given for the two extreme cases. The assumption of having a normal shock at the leading edge ("blunt" case) yields results that differ only about 10 percent from those obtained by assuming an oblique shock ("sharp" case). Although the oblique-shock assumption gives the most conservative (higher) values, the normal-shock assumption was used for both blunt leading edges in order to be consistent, as it is almost certain that the boundary layer is submerged in the high-entropy layer for the 1.27-cm-thick leading-edge model.

For sake of clarity here and elsewhere in the paper, the difference between "blunt" and "sharp" data (or theory) should be restated. For the sharp case, the local total pressure exterior to the boundary layer is assumed to be that behind an oblique shock whose strength will produce the local static pressure ratio p_l/p_∞ (or p_w/p_∞ since throughout this paper the pressure was assumed to be constant across the boundary layer). In the blunt case, the assumption is made that the local total pressure is equal to the stagnation pressure behind the near-normal portion of the leading-edge shock. By knowing the local total and static pressures for either case, the remaining local fluid properties

14

(exterior to the boundary layer) needed for reducing the data or computing the theory are found from the isentropic flow equations.

Basic Effects of Free-Stream Reynolds Number

Pressure distribution.- The effects of free-stream unit Reynolds number on the pressure distribution are shown in figure 19. For the largest bluntness (t = 1.27 cm), no sizable Reynolds number effects are noted, and the experimental data are somewhat overpredicted by the inviscid method employed. For the intermediate bluntness (t = 0.25 cm), significant viscous effects are present, but the linear addition of inviscid and viscid predictions yields results that compare quite favorably with the experimental data. Also, the experimental data for the sharp-leading-edge model are predicted fairly satisfactorily for the unit Reynolds number shown. However, a mental extrapolation (realizing here that the boundary-layer induced pressure varies roughly as the inverse of the square root of the Reynolds number) of the theory to the lowest unit Reynolds number shows that the data would be significantly underpredicted. The reason for this is not clear.

Heat-transfer results.- The primary effect of free-stream Reynolds number on the heat-transfer results can be seen in figure 20 where log-log plots of $N_{St,\infty}$ as a function of $R_{\infty,x}$ are presented. For the sharp leading edge (fig. 20(a)), the data exhibit the conventional behavior for this general range of Reynolds number, that is, from laminar to transitional to turbulent. The laminar data are approximately 20 percent higher than predicted by either T-prime or Van Driest's theory (ref. 27). However, the turbulent data are lower than predicted by Van Driest's turbulent theory[*] (ref. 28), but agree quite well with the T-prime estimates provided that the virtual origin is taken near the end of transition. The transition Reynolds number itself generally increases slightly with unit Reynolds number. Since the transition process occurs over a distance of many boundary-layer thicknesses, it is somewhat ambiguous to talk of a transition Reynolds number (or transition point). For descriptive purposes, however, some convenient arbitrary point in the transitional region is usually defined as the transition point. The particular point chosen may vary from one investigation to another, depending upon the type of data being obtained. The transition Reynolds number (or transition point) used herein is illustrated in the following sketch:

---

[*]In applying Van Driest's turbulent theory, von Kármán's mixing length was used.
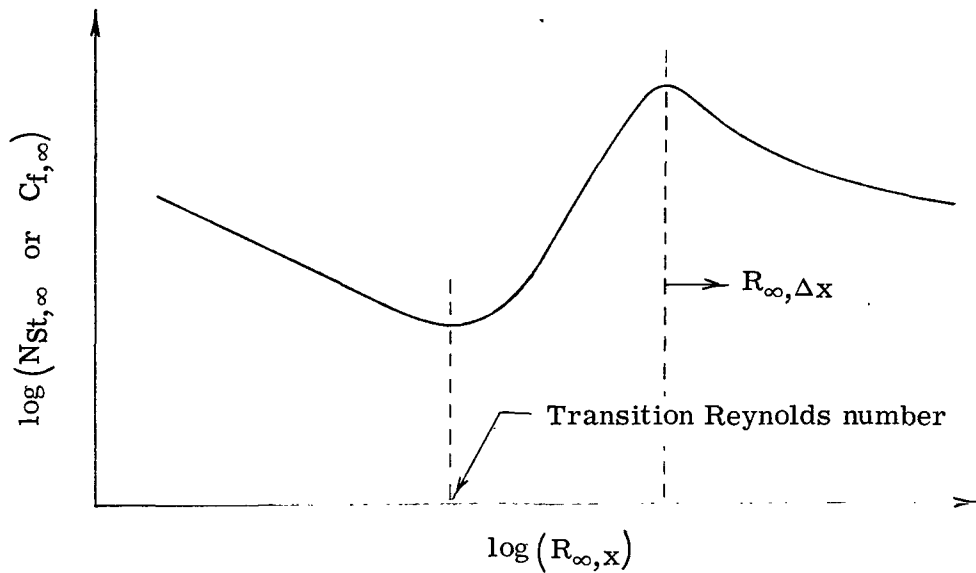
With this definition, the transition Reynolds number from the sharp-leading-edge heat-transfer results is approximately 1.5 million.

Moderate blunting (fig. 20(b)) increases the transition Reynolds number, as no signs of transition have appeared for free-stream Reynolds numbers up to about 4 million. However, for larger blunting (fig. 20(c)), transition occurs between free-stream Reynolds numbers of about 1 and 2 million, which is of the same order of magnitude as that for the sharp leading edge. This was somewhat unexpected in light of the fact that the local Reynolds number is roughly an order of magnitude less than that for the sharp leading edge. Furthermore, the transitional region has a somewhat different general appearance than that commonly noted for sharp-leading-edge models as can be seen by comparing the data points in the transitional regions shown in figures 20(a) and 20(c). However, if a line of constant pressure ratio is followed for the blunt leading edge, as indicated by the dash-dot line in figure 20(c), then the conventional type of curve is obtained. Perhaps this can be seen more clearly in figure 21 where $N_{St,\infty}$ is given as a function of $R_{\infty,x}$ for various values of p_w/p_∞. Also seen in figure 21, as the local Mach number increases (decreasing p_w/p_∞), the transitional Reynolds number increases and the amount of underestimation by the laminar theory also increases. In this figure, each value of p_w/p_∞ corresponds to a certain x-location along the model. Thus, the Reynolds number is varied by changing the unit Reynolds number. Also, the pressure gradient is constant for each plot but varies from one plot to another.

Skin-friction results.- Figure 22(a) shows the variation of $C_{f,\infty}$ with $R_{\infty,x}$ for the sharp leading edge. Practically all the data shown in the figure were taken at 20 seconds after the start of a test run. Most of the laminar runs were terminated at

20 seconds, as the output remained essentially constant after initial nullment of the recording instruments. However, there was some variation of $C_{f,\infty}$ with time in the transitional and early turbulent regions. In the transitional region, there was a noted tendency for retardation of transition as time increased. Figures 22(b) and (c) show the variation of $C_{f,\infty}$ with $R_{\infty,x}$ for the two blunt leading edges. In contrast to the sharp-leading-edge data, no significant variation of $C_{f,\infty}$ with time was observed for these blunt leading edges.

As mentioned previously, no corrections have been applied to the data due to presence of the gap associated with the floating skin-friction element, because detailed information necessary for determining such corrections has not been obtained to date. A few past users of skin-friction balances have attempted to critically evaluate the gap effect for their test environments; their resulting findings ranged from almost zero to several percent of the actual skin friction. (See, for example, refs. 18, 19, and 29.) For cases of near-zero pressure gradients, the gap effect was usually found to be small. Thus, for the present investigation, it is felt that gap effects for the sharp-leading-edge data are negligible because of the near-zero pressure gradient. (See fig. 19.) As the leading-edge bluntness increases, the surface pressure gradient likewise increases, and hence the gap effect would also be expected to increase. Therefore, the skin-friction data presented in this report must be viewed in light of these facts. In addition to the gap effect itself, there is also the effect of patch misalinement to consider; however, during the discussion of the skin-friction balance, it was concluded that errors due to this source would be expected to be on the order of 1 percent or less.

Insofar as the general overall behavior of the data is concerned, the skin-friction results are similar to the heat-transfer results presented in the previous section. One of the important results from this friction data is a verification of the suggested data behavior in the transitional region for the 1.27-cm-thick leading edge as found from the heat-transfer results. No noticeable difference in the magnitude of the transitional Reynolds number itself is found between the skin-friction and heat-transfer results for the same chordwise stations. However, the average transitional Reynolds number for the sharp leading edge is approximately 2 million, which is higher than that obtained from the heat-transfer results using the large heat-transfer panel insert. This difference in transition Reynolds number is not attributed to the method of detection, but probably to small differences in leading-edge thickness, as two different sharp leading edges were used. The dummy skin-friction insert panel, which was instrumented with five thermocouples and which made up one of the filler panels for most of the skin-friction test runs, indicated transitional Reynolds numbers which agreed with those obtained from the skin-friction results.

For the sharp leading edge, similar agreement, or disagreement, between the skin-friction data and the various theoretical estimates is seen in figure 22(a), as was noted

previously in the discussion of the heat-transfer results. However, for the blunt-leading-edge data, no meaningful comparison can be made between the actual magnitude of the data and the theories because of the unknown gap effects.

Evaluation of the Relation Between Skin Friction and Heat Transfer

One of the primary objectives of the present investigation was to find out how well the heat-transfer and skin-friction data agreed when compared through the use of the Reynolds analogy concept. The comparison of the sharp-leading-edge data is made in figure 23(a). In the laminar comparison the Colburn relation $N_{St,l} = C_{f,l}/2N_{Pr}^{2/3}$ was employed to convert measured Stanton numbers to equivalent skin-friction coefficients. (The Prandtl numbers appearing in this relation as well as those appearing in the various T-prime equations employed were evaluated at the appropriate T-prime temperatures.) The agreement is quite good; however, both are higher than theory by about 20 percent. For the turbulent comparison, von Kármán formulation combined with T-prime theory (ref. 30) was used. Again, the comparison is very good. Although the data agree fairly well with the various theoretical estimates, Spalding and Chi's method (ref. 31) appears to give the best prediction.

It should be recalled that the virtual origin was taken to be at the peak heating or shearing values at the end of transition. This same location has also been used by previous investigators (refs. 18 and 29) in presenting their data. Other locations were investigated for the present data as well as data from several other sources with the net result that selection of this peak location as the virtual origin yielded the best overall correlation with theory. Further discussion of this matter is presented in reference 30.

A comparison of the blunt-leading-edge results, obtained by the same method of conversion as that used for the sharp leading edge, is shown in figures 23(b) and 23(c). Each figure consists of four parts; in the top two a normal shock at the leading edge was assumed and in the bottom two an oblique shock at the leading edge was assumed. The right side of each figure was adjusted for the effect of pressure gradient by using the method of reference 13. Since $K_1 \approx 1$, this adjustment was made simply by dividing the heat-transfer data by the nominal values of K_3 shown in the figures. As mentioned previously, gap effects are almost certain to be present in the skin-friction data, because of the existence of a sizable pressure gradient, which makes it difficult to obtain sound conclusions in regard to the Reynolds analogy factor. Nevertheless, for completeness, these comparisons are included but without discussion.

Effects of Leading-Edge Thickness on Transitional Reynolds Number

As mentioned previously, natural transition was not expected for the blunt leading edges at the Reynolds number range of this investigation. Hence, because of the

attainment of transition for the 1.27-cm-thick leading edge, it appeared appropriate to provide additional variation in leading-edge thickness in order to establish the trend of transitional Reynolds number with leading-edge thickness. Accordingly, the program was extended in that skin-friction measurements were made for leading-edge thicknesses of 0.013 and 1.60 cm under limited test conditions. As expected, the results showed that the 0.013-cm-thick leading edge delayed transition when compared with the 0.0025-cm thickness. The boundary layer was still laminar at the maximum attainable Reynolds number of about 9 million. From the correlations presented in reference 32, the increase in transitional Reynolds number over that for $t = 0.0025$ cm would be expected to be on the order of 2 million, which would give a transitional Reynolds number of only around 4 million. The 1.60-cm-thick leading edge was tested with the balance located only at the station $x = 24.06$ cm. The transition Reynolds number was found to be about 1.3 million as compared with 1.7 million for $t = 1.27$ cm at this same station. In this particular case, transition for both leading edges occurred at practically the same bluntness Reynolds number $\left(\left(R_{\infty,t}\right)_{tr} \approx 85\ 000\right)$.

The auxiliary skin-friction data for the 0.013- and 1.60-cm-thick leading edges are given in figure 24.

It should be mentioned that in the transition study at Mach 3.1 reported in reference 33, the bluntness shape, that is, flat or rounded, was discovered to have significant effect on transition, depending on the value of the bluntness Reynolds number. For a bluntness Reynolds number greater than about 20 000 (for the hollow cylinder), it was found that flat bluntness had a detrimental effect on transition. This reverse trend in transition Reynolds number as leading-edge thickness (flat bluntness) is increased is thus in agreement with the present results for flat bluntness.

CONCLUSIONS

A study of the pressure, heat-transfer, and skin-friction distributions over a flat plate with both sharp and blunt leading edges has been conducted at a nominal free-stream Mach number of 6.8, over a range of free-stream Reynolds numbers per centimeter from about 0.02×10^6 to 0.16×10^6, and at a wall-to-stagnation temperature ratio of about 0.5. The model consisted of a 25.4-cm-wide by 61-cm-long flat plate equipped with interchangeable leading edges having thicknesses of 0.0025, 0.25, and 1.27 cm. The investigation covered all three flow regimes — laminar, transitional, and turbulent. Analysis of the experimental results yielded the following conclusions:

1. There was no significant effect of unit Reynolds number on the pressure distribution for the 1.27-cm-thick leading edge for surface distances up to about 20 times the leading-edge thickness. However, for the 0.25-cm-thick leading edge, viscid effects were obtained, which were roughly of the same order of magnitude as those found for the

"sharp" (0.0025 cm thick) leading edge. The agreement between theoretical and experimental pressures could be classified as fair to good for the particular theories employed except for the following cases. The pressure for the 1.27-cm-thick leading edge decayed faster than that indicated by theory, and significant overprediction of experimental results occurred at large streamwise distances from the leading edge. Also, the pressure for the sharp leading edge at the lowest unit Reynolds number was significantly and inexplicably higher than predicted.

2. By taking the virtual origin at the point of peak shear stress (or heating) at the end of transition, the turbulent skin-friction data for the sharp leading edge were satisfactorily predicted. However, the laminar skin-friction data for this same leading edge were about 20 percent higher than indicated by theory. For the blunt leading edges, no meaningful comparison could be made between the actual level of the skin-friction data and theory because of the unknown magnitude of the skin-friction balance gap effects. These effects were almost certain to be present because of the existence of a sizable pressure gradient associated with the blunt leading edges.

3. For the sharp leading edge, the heat-transfer data agreed with theory in a fashion similar to that noted in conclusion 2 for the skin-friction data. The laminar heat-transfer data for the blunt leading edge agreed fairly well with zero-pressure-gradient theory but were underpredicted when pressure-gradient effects were taken into account. The small quantity of turbulent heat-transfer data obtained for the blunt leading edge appeared to be overpredicted.

4. For the sharp leading edge, good agreement between measured skin-friction and heat-transfer results was obtained, for both laminar and turbulent flow, with use of the Colburn relation and the von Kármán form of the Reynolds analogy combined with the T-prime theory, respectively. For the blunt leading edges, however, no sound conclusion regarding the Reynolds analogy could be made because of the unknown magnitude of the skin-friction balance gap effect.

5. Small and moderate leading-edge blunting delayed transition whereas large blunting produced about the same transition Reynolds number as the sharp leading edge.

6. The results indicated only a small effect of unit Reynolds number on the transition Reynolds number for the sharp leading edge.

Langley Research Center,
National Aeronautics and Space Administration,
Langley Station, Hampton, Va., September 2, 1965.

REFERENCES

1. Bertram, Mitchel H.: Viscous and Leading-Edge Thickness Effects on the Pressures on the Surface of a Flat Plate in Hypersonic Flow. J. Aeron. Sci. (Readers' Forum), vol. 21, no. 6, June 1954, pp. 430-431.

2. Bertram, Mitchel H.: An Approximate Method for Determining the Displacement Effects and Viscous Drag of Laminar Boundary Layers in Two-Dimensional Hypersonic Flow. NACA TN 2773, 1952.

3. Lees, Lester; and Probstein, Ronald F.: Hypersonic Viscous Flow Over a Flat Plate. Rept. No. 195 (Contract AF 33(038)-250), Aeron. Eng. Lab., Princeton Univ., Apr. 20, 1952.

4. Lees, Lester: Influence of the Leading-Edge Shock Wave on the Laminar Boundary Layer at Hypersonic Speeds. J. Aeron. Sci., vol. 23, no. 6, June 1956, pp. 594-600, 612.

5. Bertram, Mitchel H.: Boundary-Layer Displacement Effects in Air at Mach Numbers of 6.8 and 9.6. NASA TR R-22, 1959. (Supersedes NACA TN 4133.)

6. Cheng, H. K.; and Pallone, A. J.: Inviscid Leading-Edge Effect in Hypersonic Flow. J. Aeron. Sci. (Readers' Forum), vol. 23, no. 7, July 1956, pp. 700-702.

7. Lees, Lester; and Kubota, Toshi: Inviscid Hypersonic Flow Over Blunt-Nosed Slender Bodies. J. Aeron. Sci., vol. 24, no. 3, Mar. 1957, pp. 195-202.

8. Bertram, M. H.; and Baradell, D. L.: A Note on the Sonic-Wedge Leading-Edge Approximation in Hypersonic Flow. J. Aeron. Sci. (Readers' Forum), vol. 24, no. 8, Aug. 1957, pp. 627-629.

9. Baradell, Donald L.; and Bertram, Mitchel H.: The Blunt Plate in Hypersonic Flow. NASA TN D-408, 1960.

10. Hammitt, Andrew G.: The Hypersonic Viscous Effect on a Flat Plate With Finite Leading Edge. Rept. No. 378 (WADC TN 57-105), Dept. Aeron. Eng., Princeton Univ., Mar. 1957.

11. Bertram, Mitchel H.; and Blackstock, Thomas A.: Some Simple Solutions to the Problem of Predicting Boundary-Layer Self-Induced Pressures. NASA TN D-798, 1961.

12. Cheng, Hsien K.: Hypersonic Flow With Combined Leading-Edge Bluntness and Boundary-Layer Displacement Effect. Rept. No. AF-1285-A-4 (Contract Nonr-2653(00)), Cornell Aeron. Lab., Inc., Aug. 1960.

13. Bertram, Mitchel H.; and Feller, William V.: A Simple Method for Determining Heat Transfer, Skin Friction, and Boundary-Layer Thickness for Hypersonic Laminar Boundary-Layer Flows in a Pressure Gradient. NASA MEMO 5-24-59L, 1959.

14. Cohen, Clarence B.; and Reshotko, Eli: Similar Solutions for the Compressible Laminar Boundary Layer With Heat Transfer and Pressure Gradient. NACA Rept. 1293, 1956. (Supersedes NACA TN 3325.)

15. Cohen, Nathaniel B.: A Method for Computing Turbulent Heat Transfer in the Presence of a Streamwise Pressure Gradient for Bodies in High-Speed Flow. NASA MEMO 1-2-59L, 1959.

16. McLellan, Charles H.; Williams, Thomas W.; and Bertram, Mitchel H.: Investigation of a Two-Step Nozzle in the Langley 11-Inch Hypersonic Tunnel. NACA TN 2171, 1950.

17. McLellan, Charles H.; Williams, Thomas W.; and Beckwith, Ivan E.: Investigation of the Flow Through a Single-Stage Two-Dimensional Nozzle in the Langley 11-Inch Hypersonic Tunnel. NACA TN 2223, 1950.

18. Coles, Donald: Measurements in the Boundary Layer on a Smooth Flat Plate in Supersonic Flow. III. Measurements in a Flat-Plate Boundary Layer at the Jet Propulsion Laboratory. Rept. No. 20-71 (Contract No. DA-04-495-Ord 18), Jet Propulsion Lab., C.I.T., June 1, 1953.

19. Shutts, W. H.; Hartwig, W. H.; and Weiler, J. E.: Final Report on Turbulent Boundary-Layer and Skin-Friction Measurements on a Smooth, Thermally Insulated Flat Plate at Supersonic Speeds. DRL-364, CM-823 (Contract NOrd-9195), Univ. of Texas, Jan. 5, 1955.

20. Tendeland, Thorval; Nielsen, Helmer L.; and Fohrman, Melvin J.: The Flow Field Over Blunted Flat Plates and Its Effect on Turbulent Boundary-Layer Growth and Heat Transfer at a Mach Number of 4.7. NASA TN D-689, 1961.

21. O'Donnell, Francis B., Jr.: A Study of the Effect of Floating-Element Misalignment on Skin-Friction-Balance Accuracy. DRL-515, CR-10 (Contract NOrd-16498), Univ. of Texas, Mar. 3, 1964.

22. Monaghan, R. J.: An Approximate Solution of the Compressible Laminar Boundary Layer on a Flat Plate. R. & M. No. 2760, British A.R.C., 1953.

23. Monaghan, R. J.: On the Behavior of Boundary Layers at Supersonic Speeds. Fifth International Aeronautical Conference (Los Angeles, Calif., June 20-23, 1955), Inst. Aeron. Sci., Inc., 1955, pp. 277-315.

24. Hilsenrath, Joseph: The NBS-NACA Tables of Thermal Properties of Gases. Table 2.44 Dry Air — Prandtl Number. National Bur. Standards, U.S. Dept. of Commerce, July 1950.

25. Holloway, Paul F.; and Sterrett, James R.: Effect of Controlled Surface Roughness on Boundary-Layer Transition and Heat Transfer at Mach Numbers of 4.8 and 6.0. NASA TN D-2054, 1964.

26. Bertram, M. H.; and Wiggs, M. Margarette: Effect of Surface Distortions on the Heat Transfer to a Wing at Hypersonic Speeds. Paper No. 62-127, Inst. Aerospace Sci., June 1962.

27. Van Driest, E. R.: Investigation of Laminar Boundary Layer in Compressible Fluids Using the Crocco Method. NACA TN 2597, 1952.

28. Van Driest, E. R.: The Problem of Aerodynamic Heating. Aeron. Eng. Rev., vol. 15, no. 10, Oct. 1956, pp. 26-41.

29. Matting, Fred W.; Chapman, Dean R.; Nyholm, Jack R.; and Thomas, Andrew G.: Turbulent Skin Friction at High Mach Numbers and Reynolds Numbers in Air and Helium. NASA TR R-82, 1961.

30. Bertram, Mitchel H.; and Neal, Luther, Jr.: Recent Experiments in Hypersonic Turbulent Boundary Layers. Presented at the AGARD Specialists Meeting on Recent Developments in Boundary-Layer Research (Naples, Italy), May 10-14, 1965.

31. Spalding, D. B.; and Chi, S. W.: The Drag of a Compressible Turbulent Boundary Layer on a Smooth Flat Plate With and Without Heat Transfer. J. Fluid Mech., vol. 18, pt. 1, Jan. 1964, pp. 117-143.

32. Potter, J. Leith; and Whitfield, Jack D.: Effects of Unit Reynolds Number, Nose Bluntness, and Roughness on Boundary Layer Transition. AEDC-TR-60-5 (Contract No. AF 40(600)-800), Arnold Eng. Dev. Center, Mar. 1960.

33. Brinich, Paul F.; and Sands, Norman: Effect of Bluntness on Transition for a Cone and a Hollow Cylinder at Mach 3.1. NACA TN 3979, 1957.
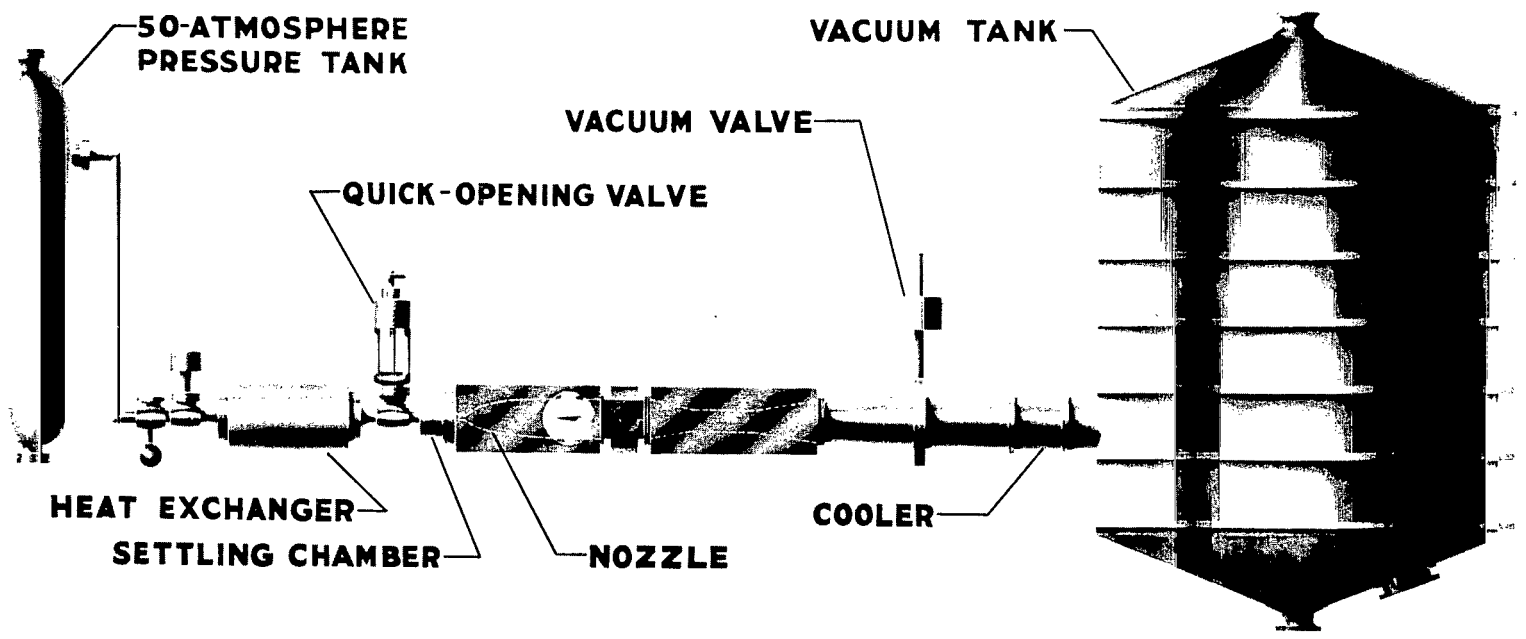
Figure 1.- Schematic of Langley 11-inch hypersonic tunnel.

X, cm

0   ○ } Present check calibration
-28 □ }
0   — 1961 calibration

τ = 20 sec

$p_t \approx 20$ atm
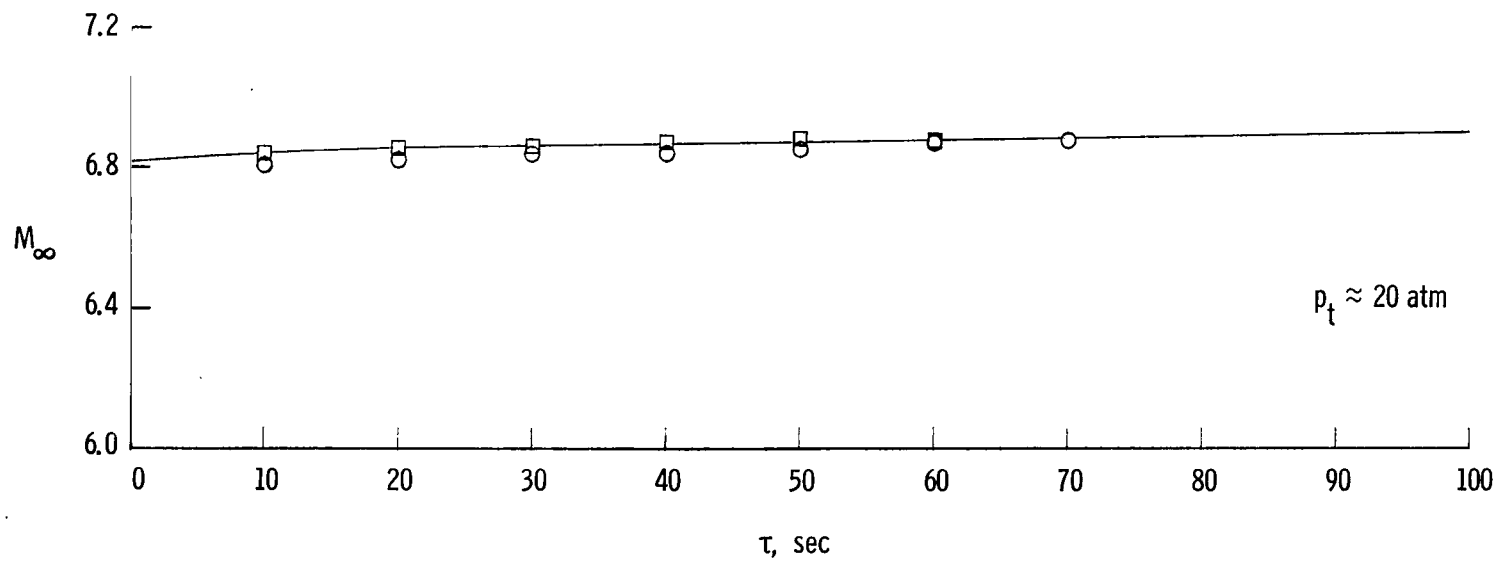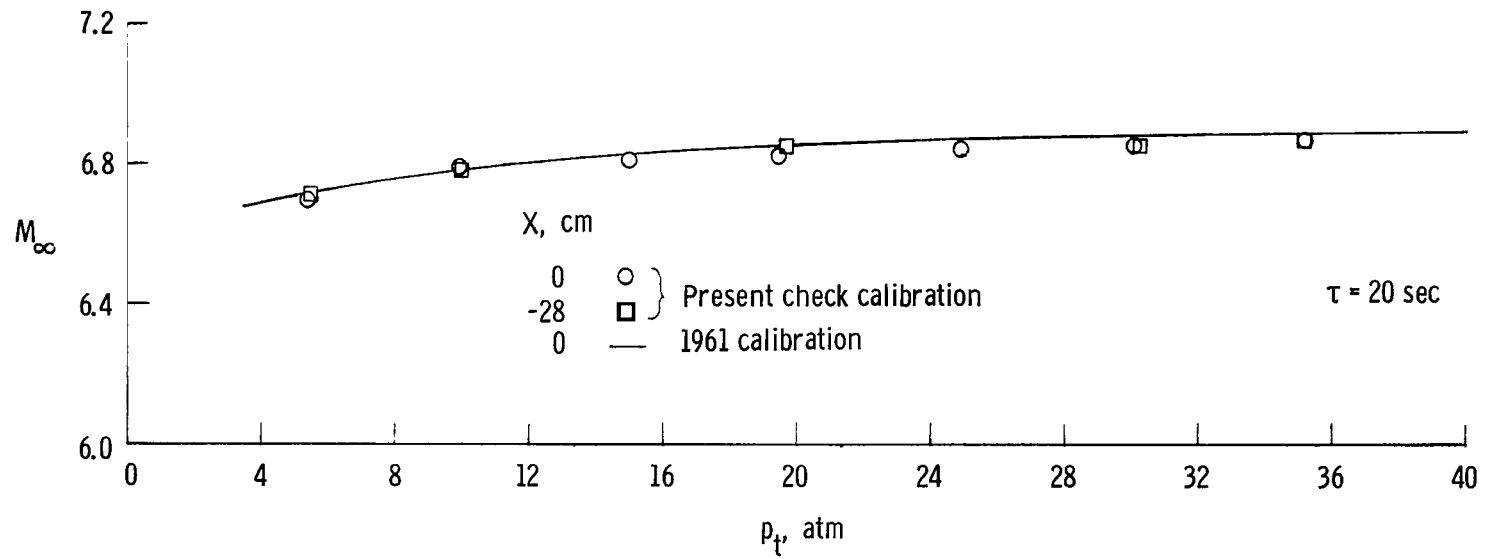
Figure 2.- Excerpts of Mach 6.8 invar nozzle calibration. $T_t \approx 610^0$ K. (Based on entire usable core size.)
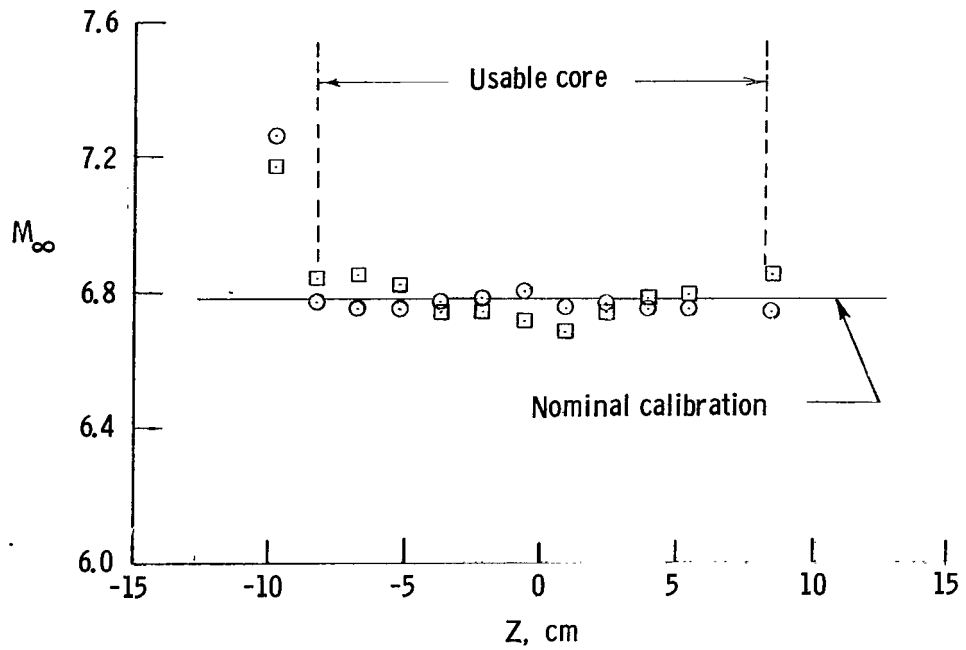
(a) Rake vertical.
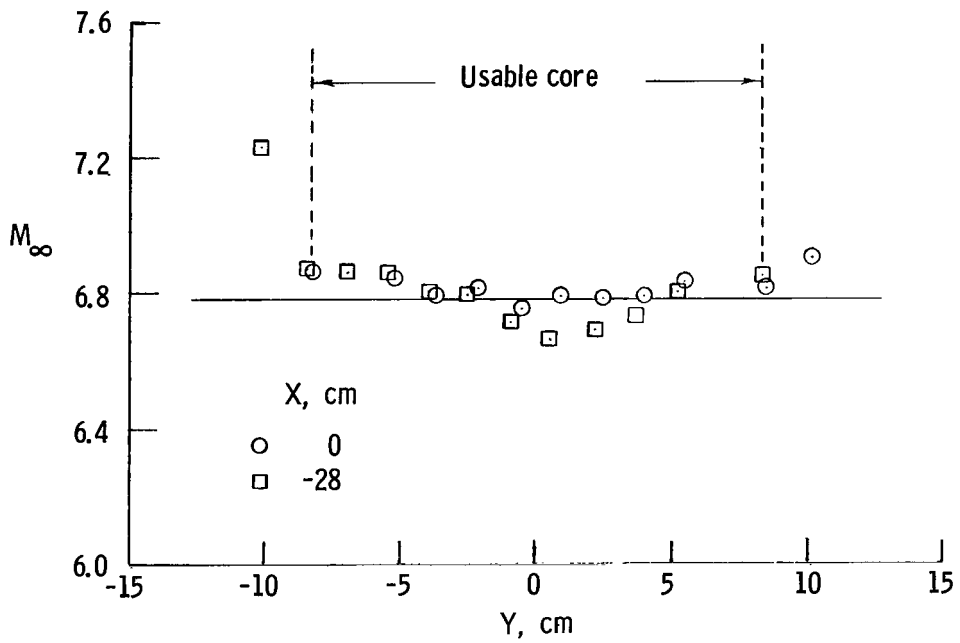
(b) Rake horizontal.

Figure 3.- Typical cross-section Mach number distribution obtained from pitot pressure measurements. $p_t \approx 10$ atm; $T_t \approx 610^\circ$ K; $\tau \approx 20$ sec.

Top of nozzle

1.27

t*

20°

A   A

X

x

x'

₵ window

window

≈ 28**

60.96

z, Z

Model support and housing'
for skin-friction balance

y, Y

Outline of nozzle at X = 0
(27.94 cm square)

48.89

10.79

25.40

Removable leading edge

Removable to facilitate
mountings of instrumented
panels as shown in figure 5

15°

4.06   5.08

Section A-A

*   t = 0.0025, 0.25, 1.27

** unless otherwise noted
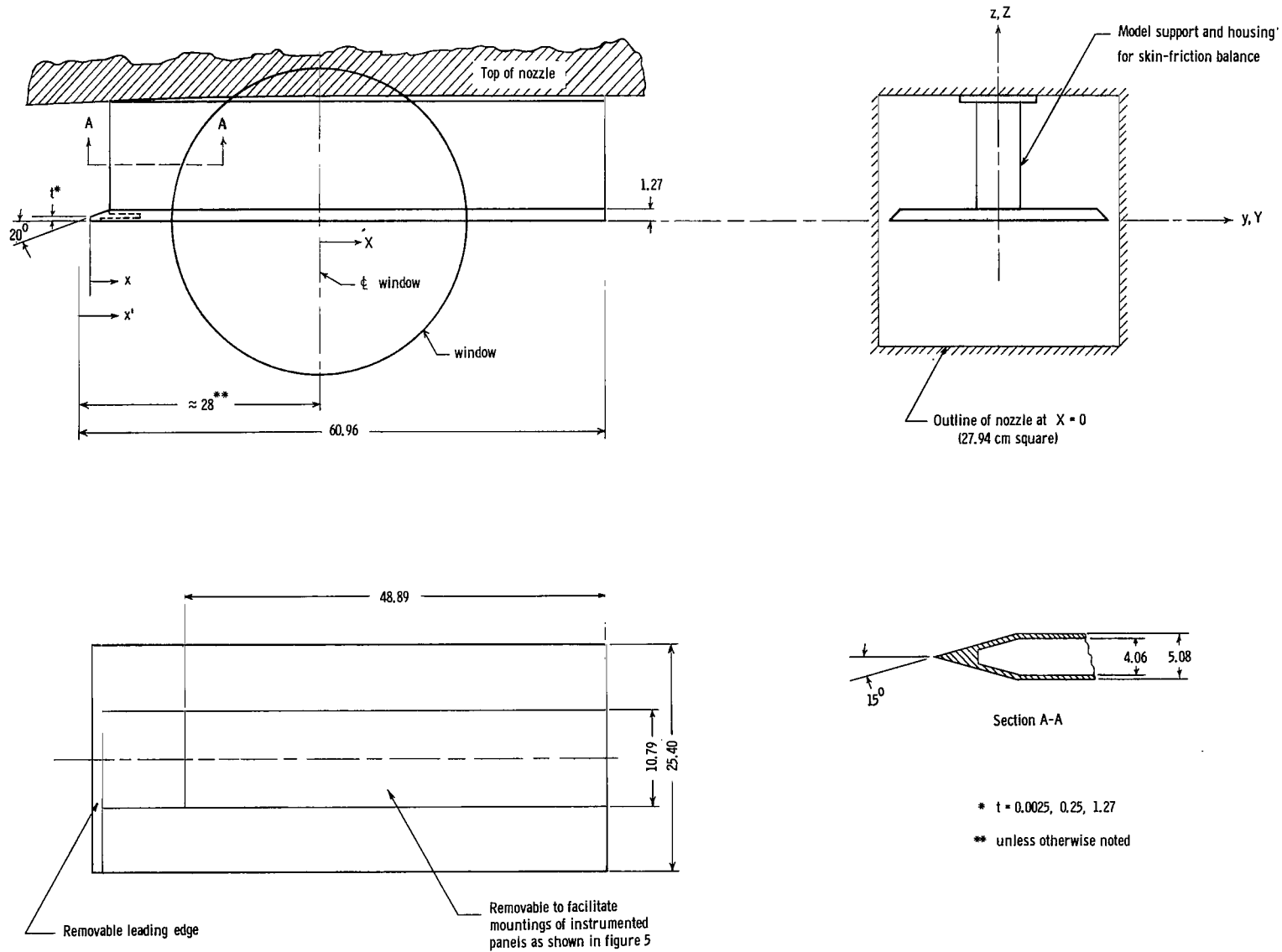
Figure 4.- Sketch of model and method of mounting in the tunnel. All dimensions are in centimeters.

0.31

48.89

1.90

10.79

3.81

x'

13.33
14.60
17.14
etc.

55.24

(a) Pressure panel insert.

0.15

0.31

48.89

1.90

10.79

3.81

x'

13.33
14.60
17.14
etc.

55.24

(b) Heat-transfer panel insert.

Skin-friction balance

Skin-friction patch

5.08

0.0025 clearance

10.79

Two pressure taps connected
to balance chamber

2.54
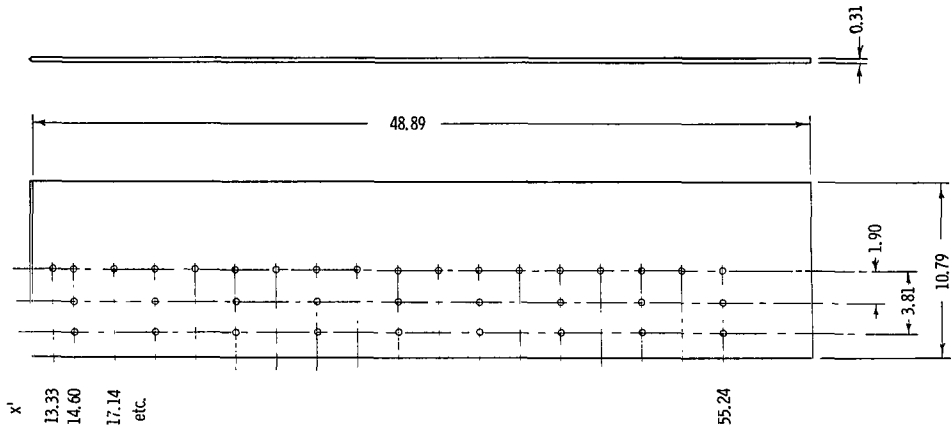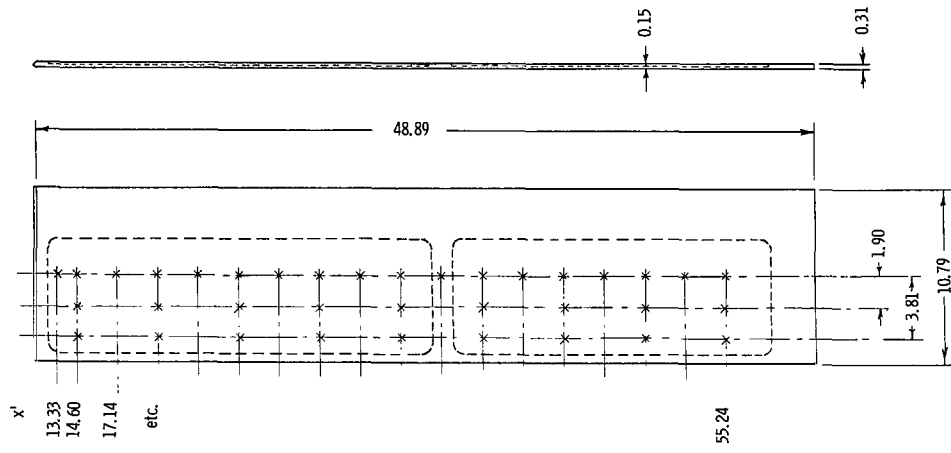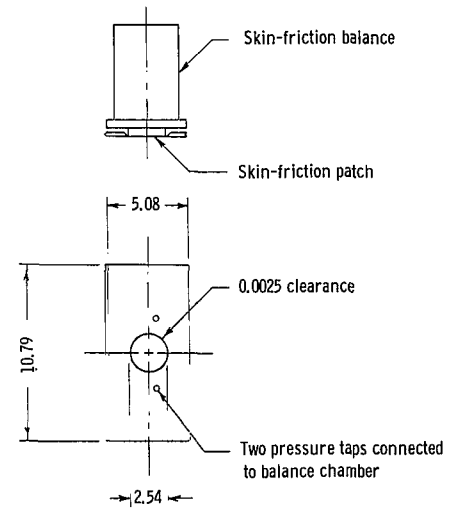
(c) Skin-friction panel insert.

Figure 5.- Sketch of the various instrumented panels. All dimensions are in centimeters.
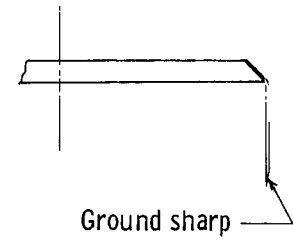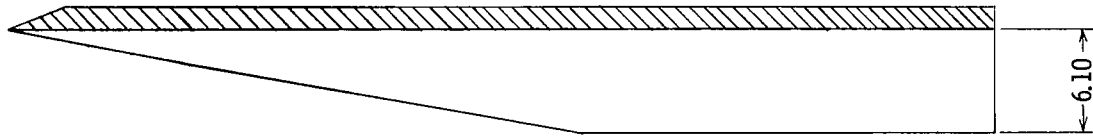
(a) Side plates for the sharp-leading-edge model.

Ground sharp
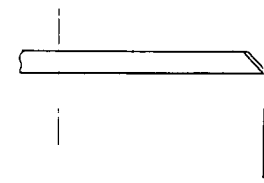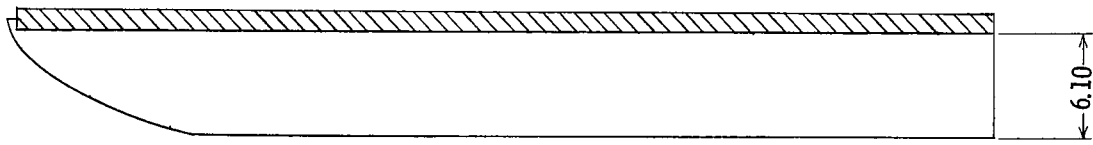
(b) Side plates for the blunt-leading-edge models.

Figure 6.- Sketch of side plates. Dimensions are in centimeters.

6.10

6.10

29
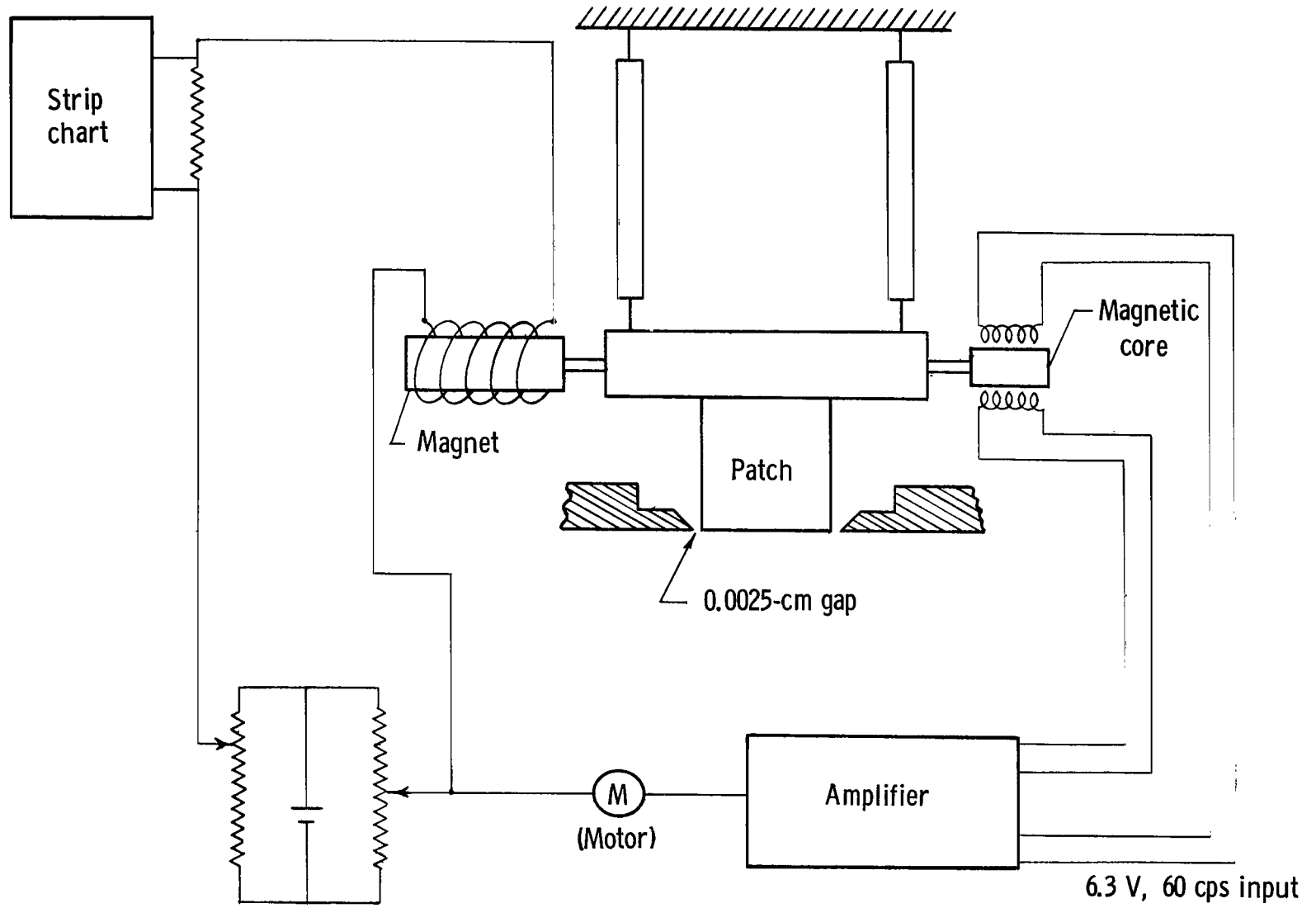
Figure 7.- Schematic of skin-friction balance.
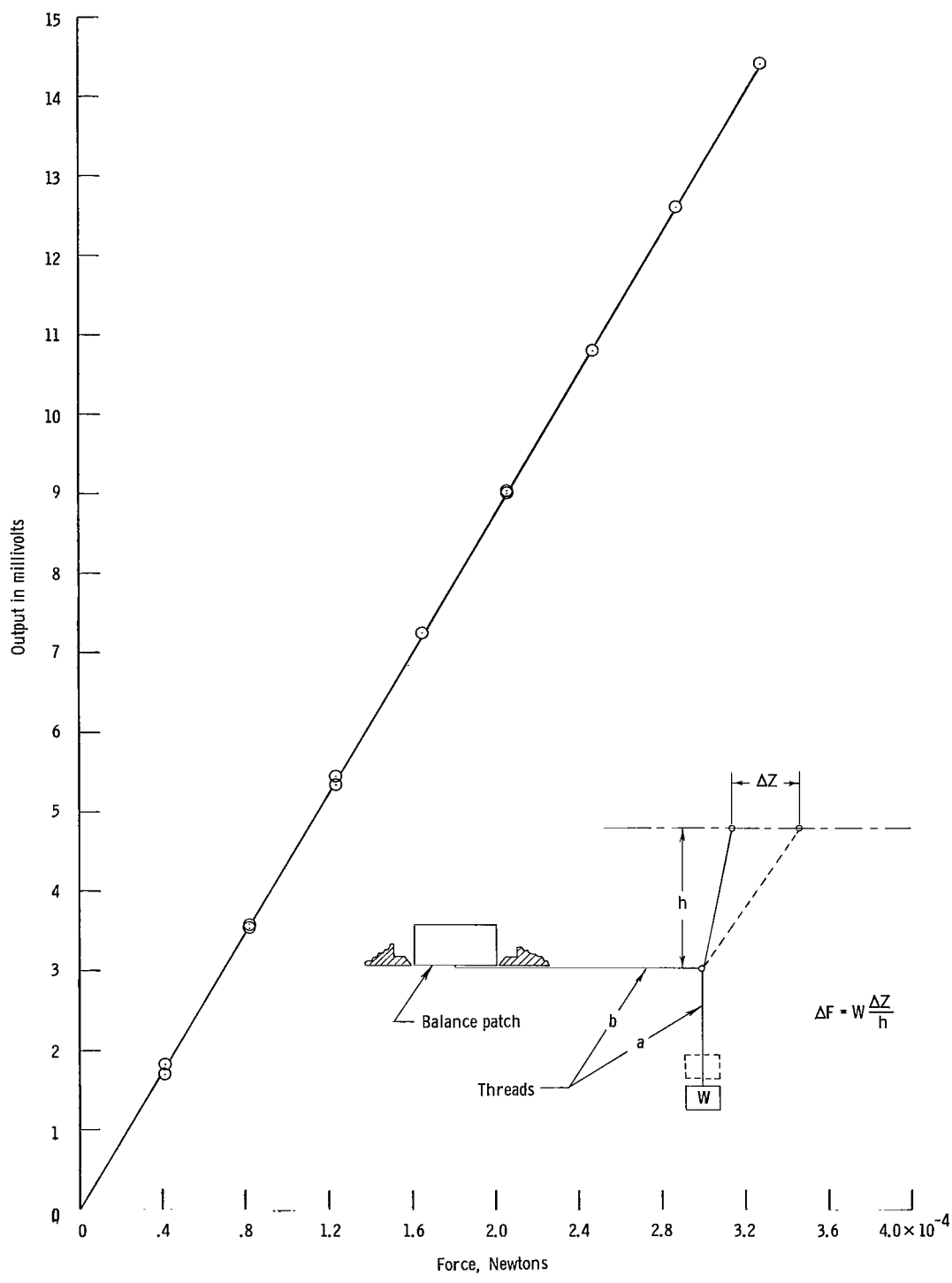
Figure 8.- Calibration of skin-friction balance.
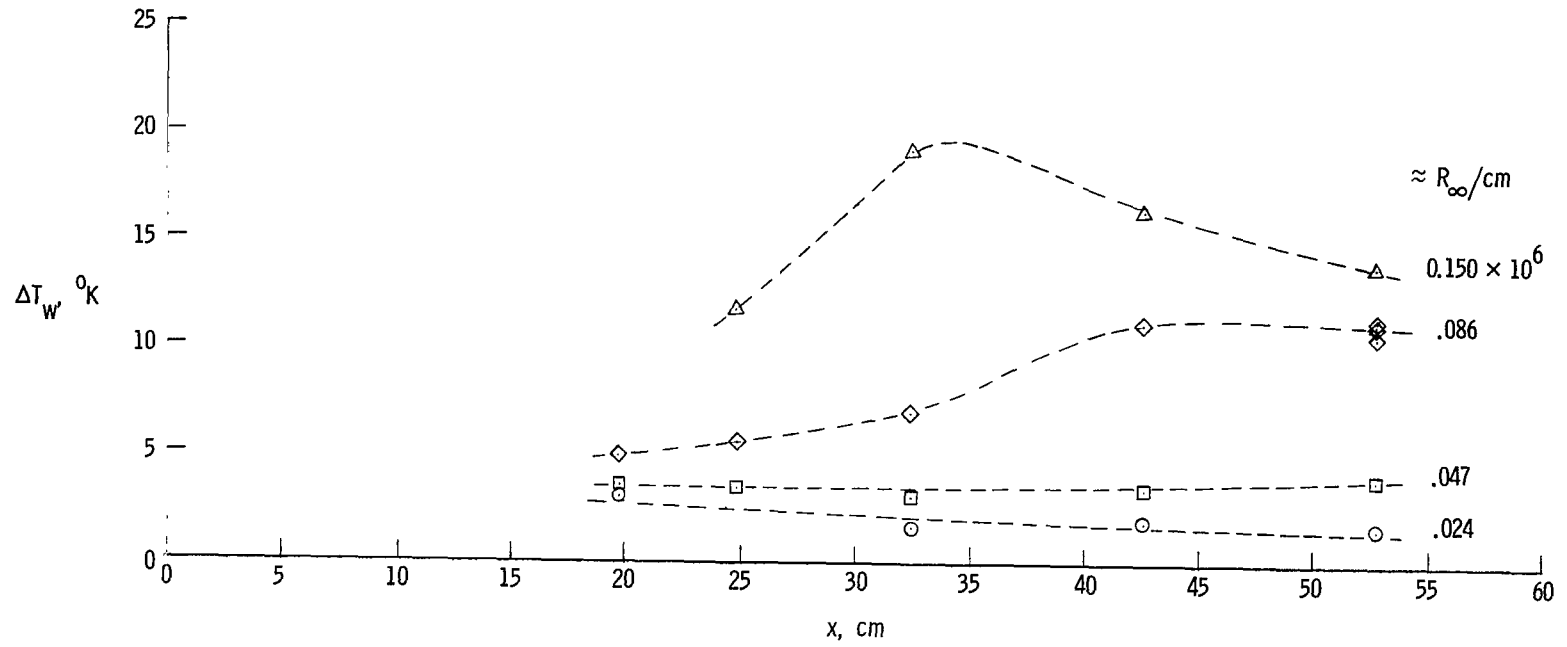
Figure 9.- Net surface temperature rise for the sharp-leading-edge model during the first 20 seconds of run.
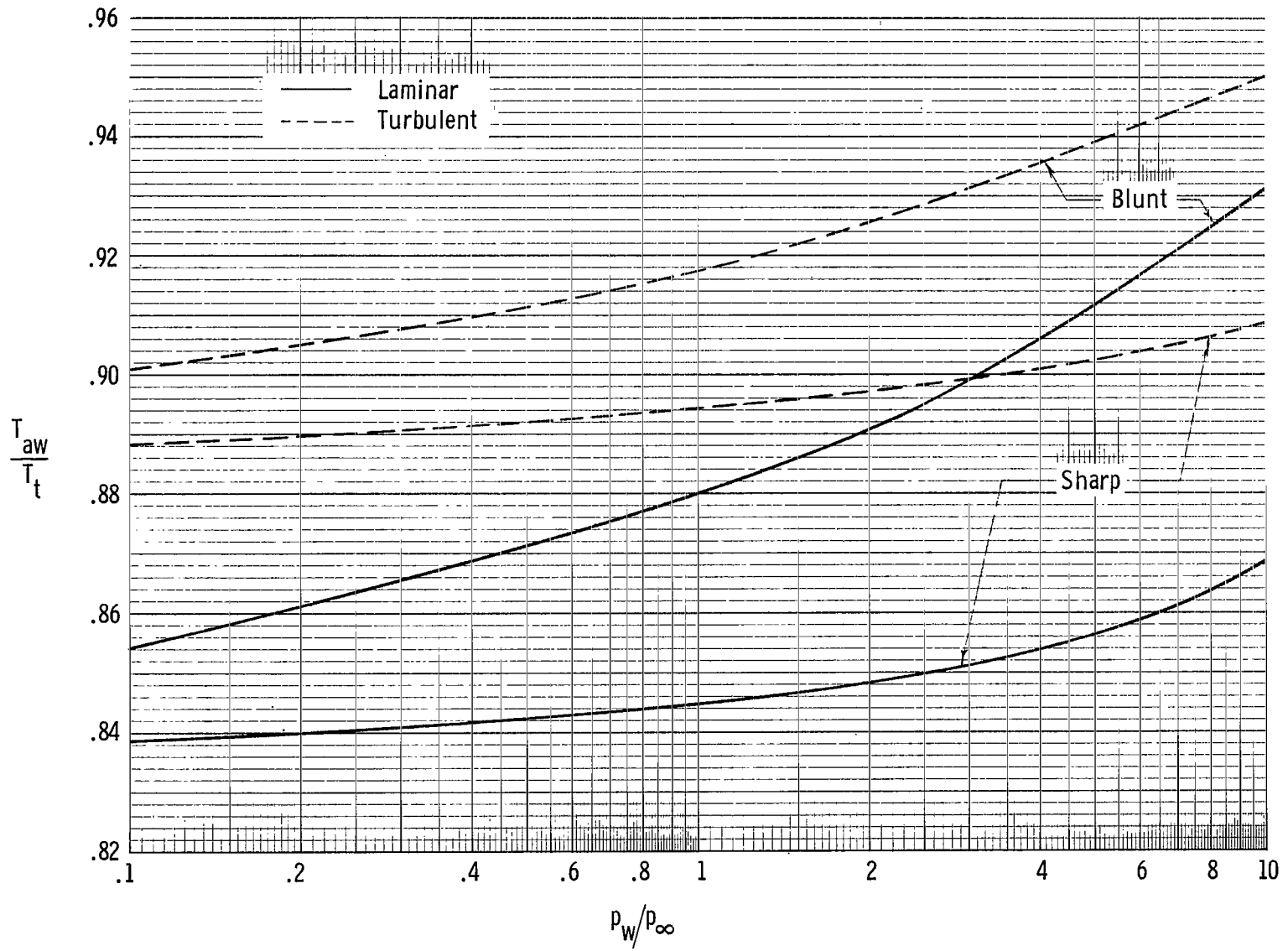
Figure 10.- Adiabatic-wall temperature used in reducing heat-transfer data. $M_\infty = 6.8$; $T_\infty = 60^0$ K.
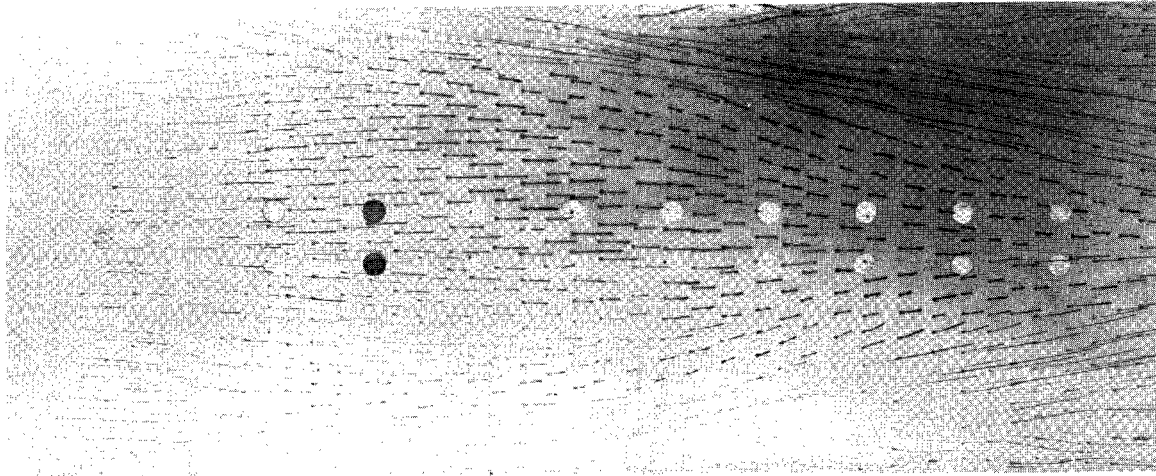
(a) Without side plates.
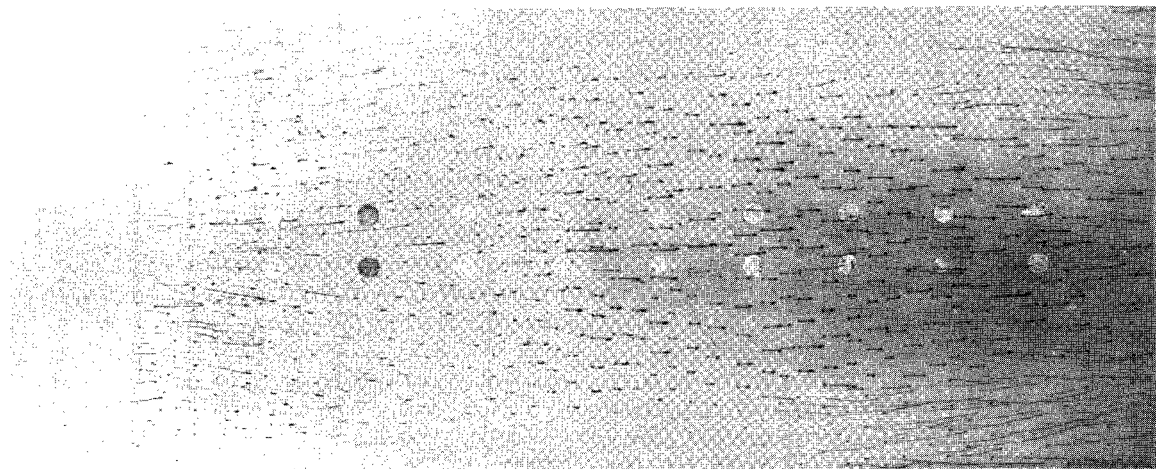
(b) With side plates.

Figure 11.- Surface flow patterns for the dummy sharp-leading-edge model. $R_\infty/cm \approx 0.15 \times 10^6$.

L-65-7925
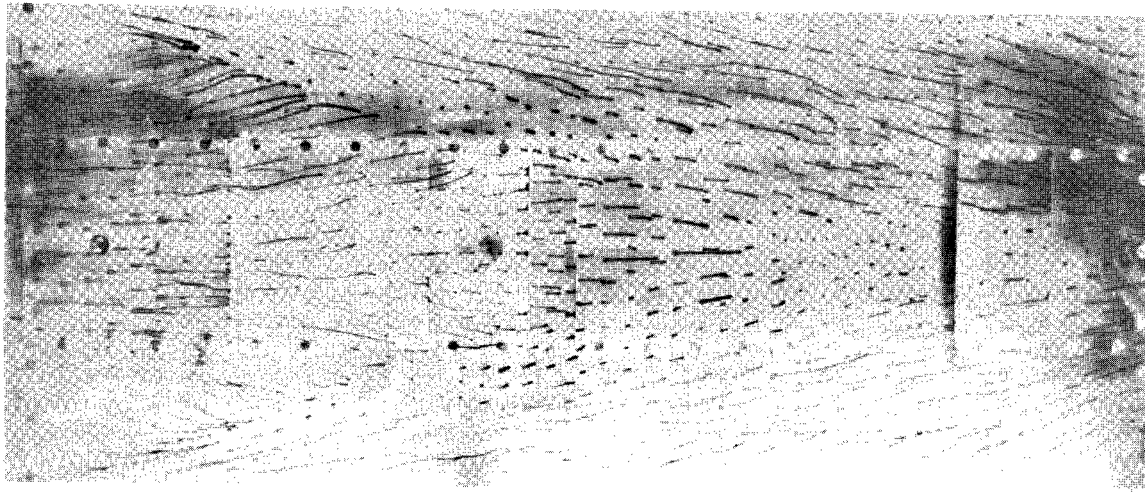
t = 1.27 cm
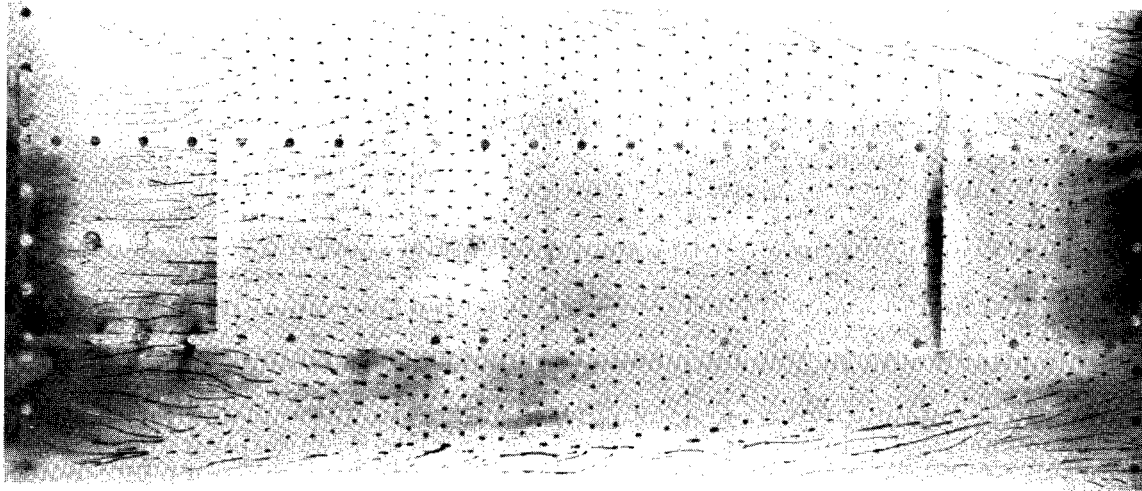
t = 0.25 cm

Figure 12.- Surface flow patterns for the blunt-leading-edge models (with side plates). $R_\infty/cm \approx 0.067 \times 10^6$.

L-65-7926
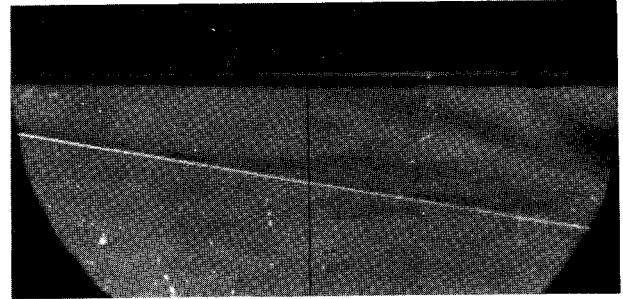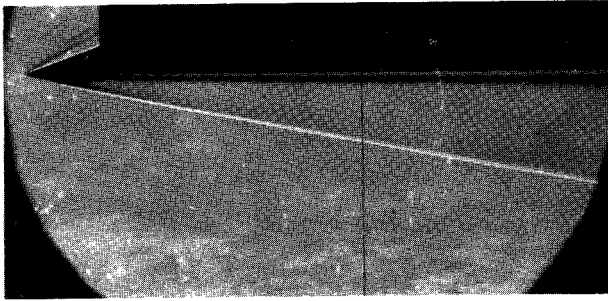
t = 0.0025 cm
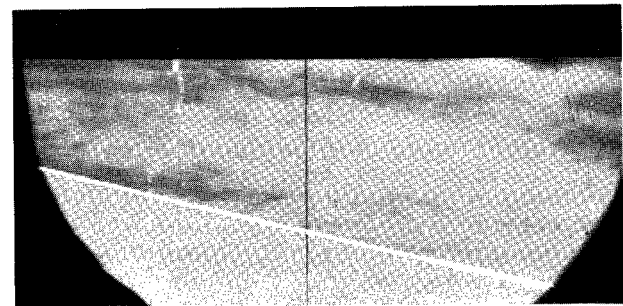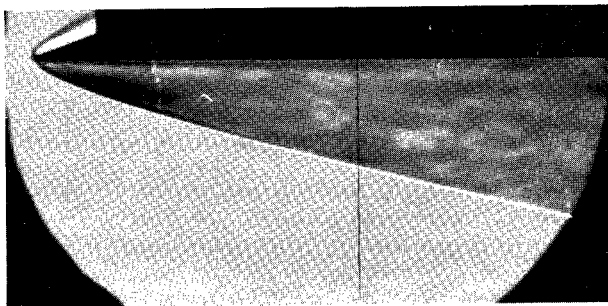
t = 0.25 cm
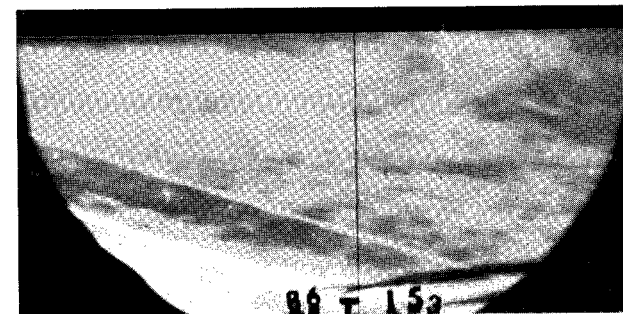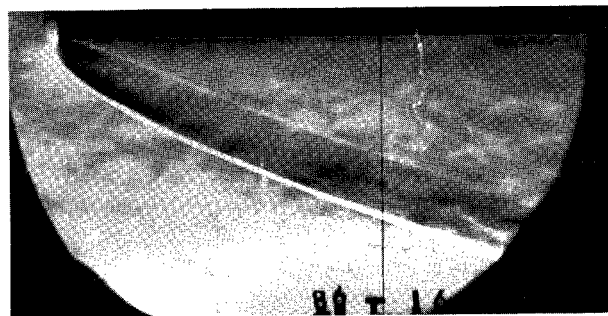
t = 1.27 cm

Figure 13.- Schlieren photographs of the model for the various leading-edge thicknesses. $R_\infty/cm \approx 0.047 \times 10^6$.   L-65-7927

36
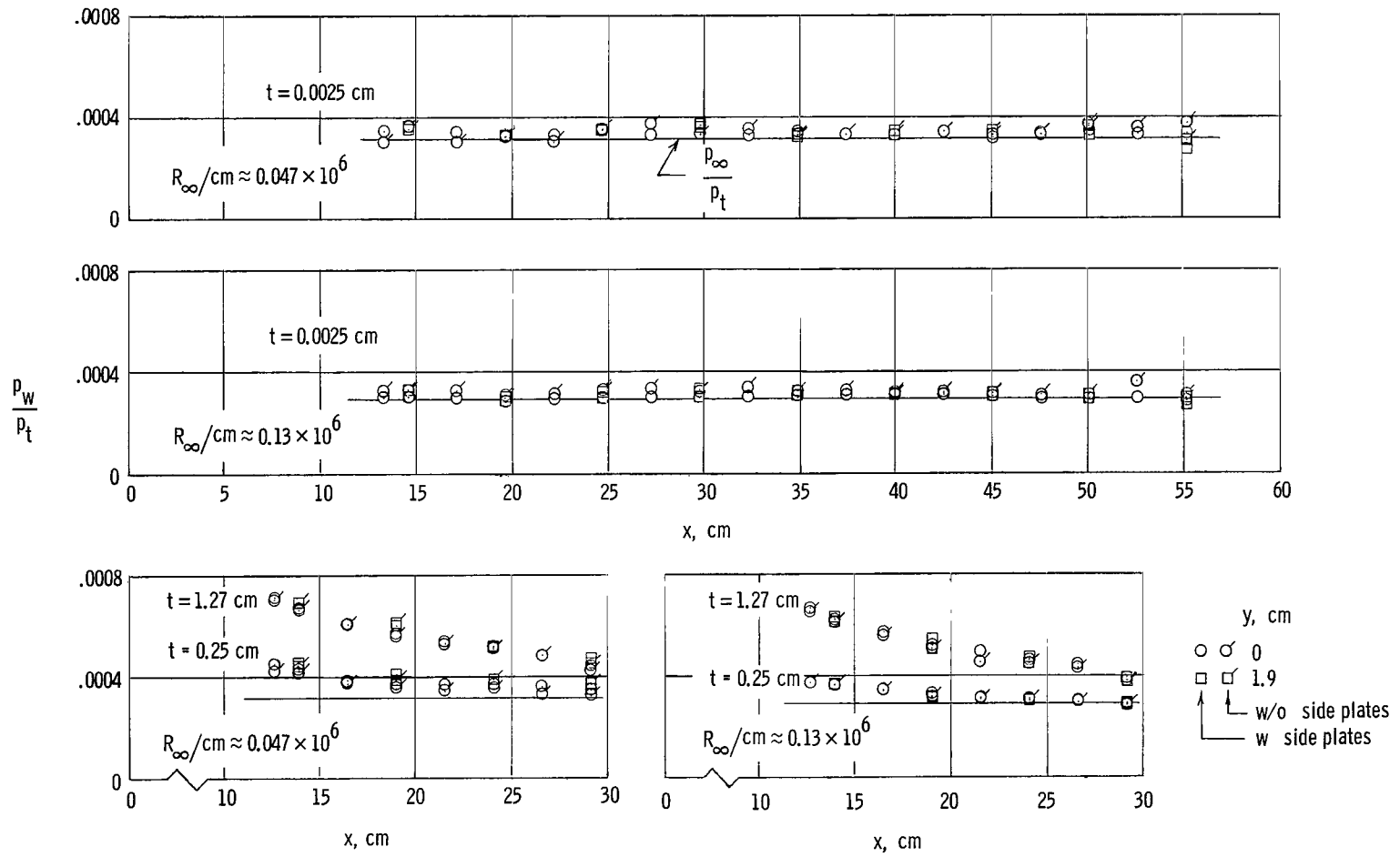
(a) Pressure.

Figure 14.- Spanwise variations and qualitative effects of side plates.
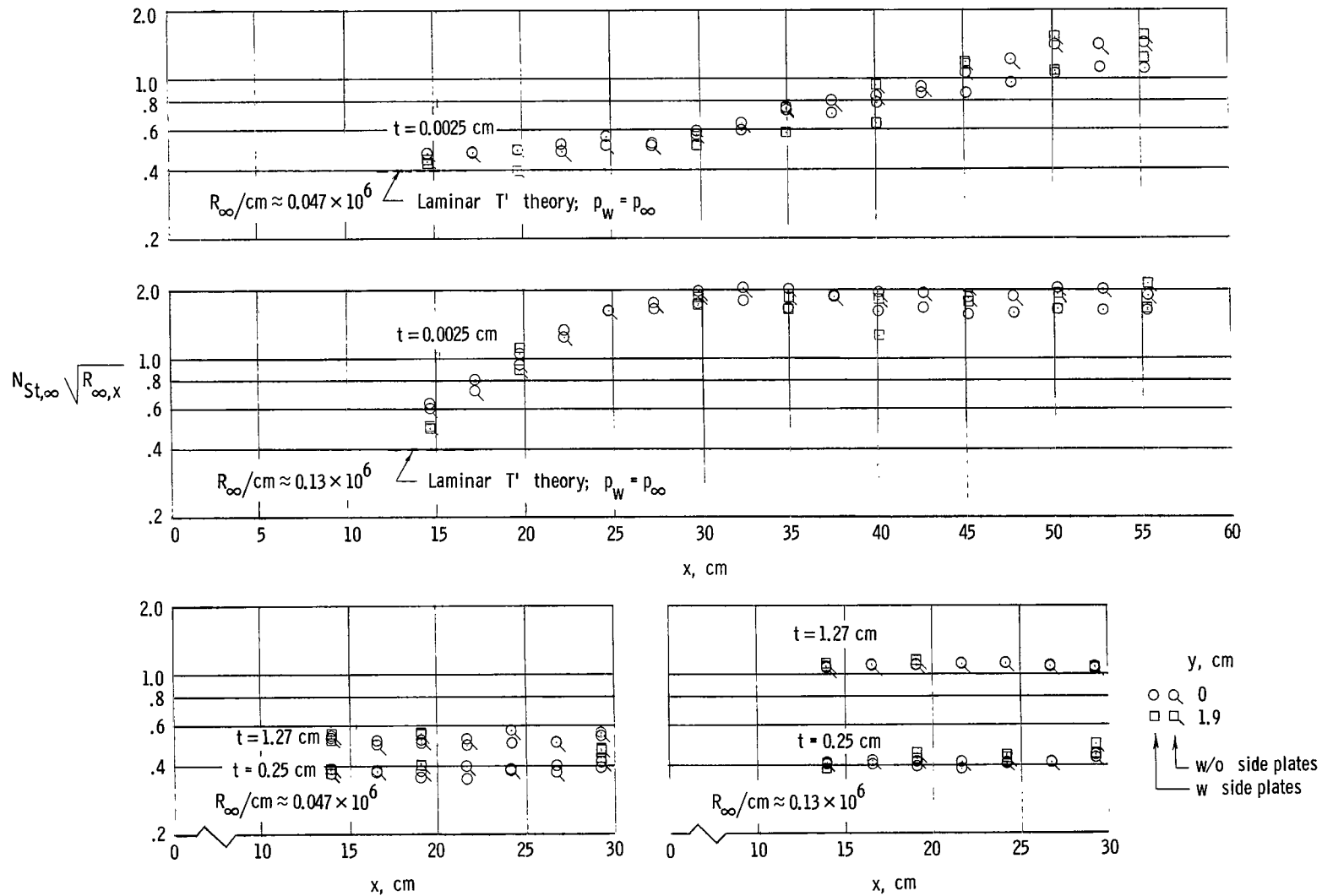
(b) Heat transfer.

Figure 14.- Concluded.
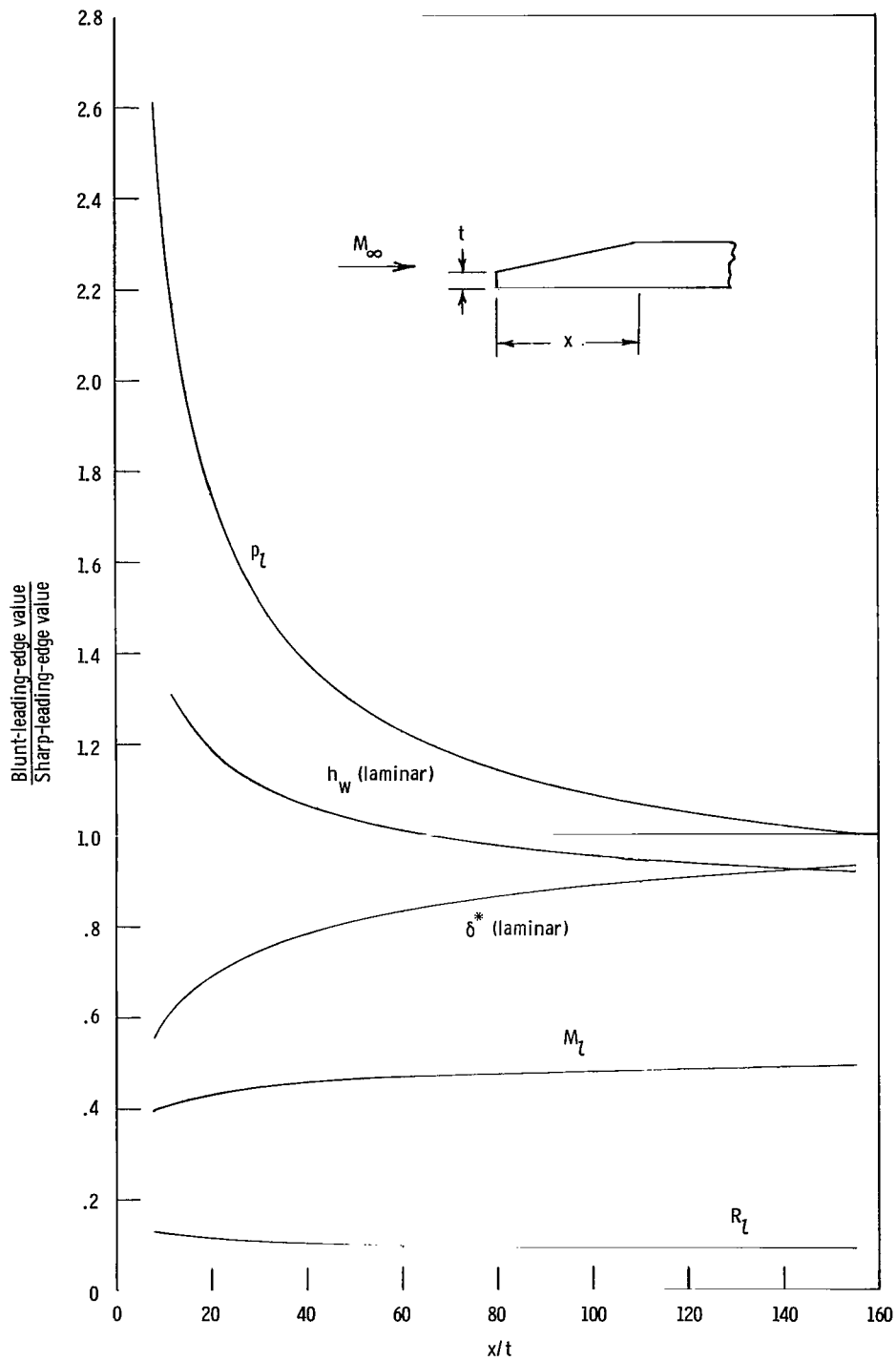
Figure 15.- Calculated ratios of blunt-leading-edge value to sharp-leading-edge value of several local-flow and boundary-layer parameters. $M_\infty = 6.8$; $T_\infty = 60^\circ$ K; $T_w = 308^\circ$ K.
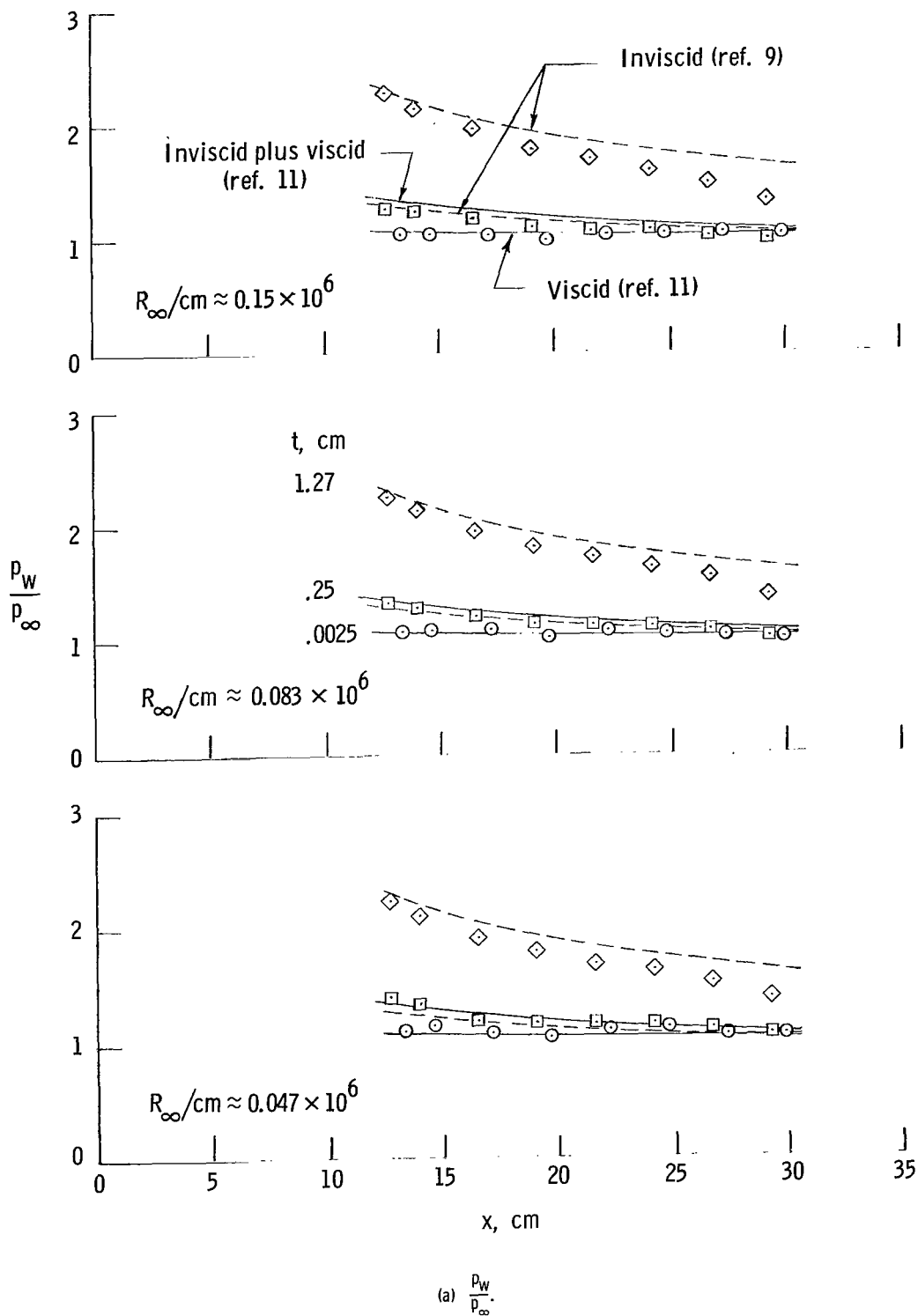
Figure 16.- Effects of leading-edge thickness on the pressure, heat transfer, and skin friction for three representative unit Reynolds numbers.

$$(a) \quad \frac{p_w}{p_\infty}.$$

40
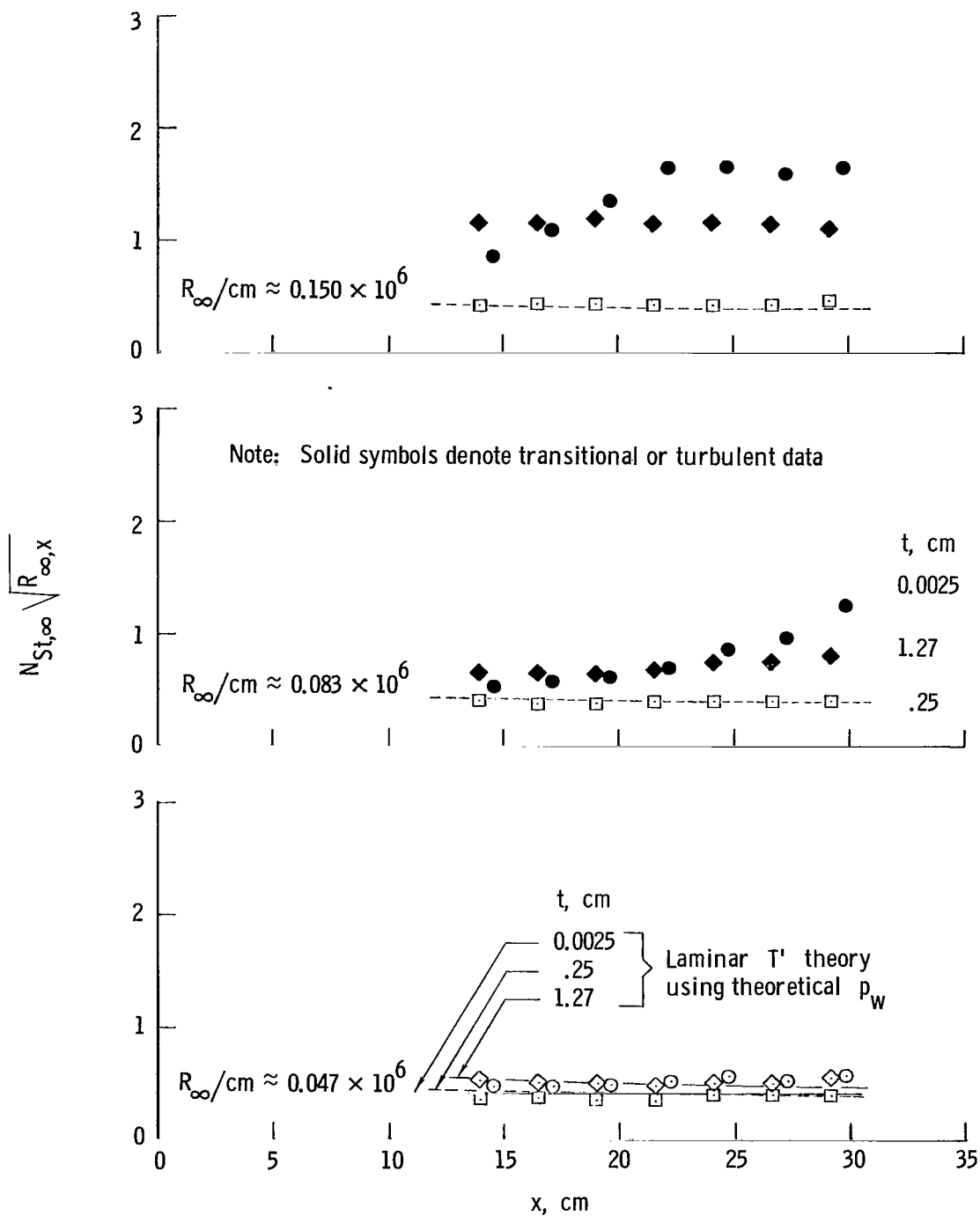
(b) $N_{St,\infty}\sqrt{R_{\infty,x}}$.

Figure 16.- Continued.
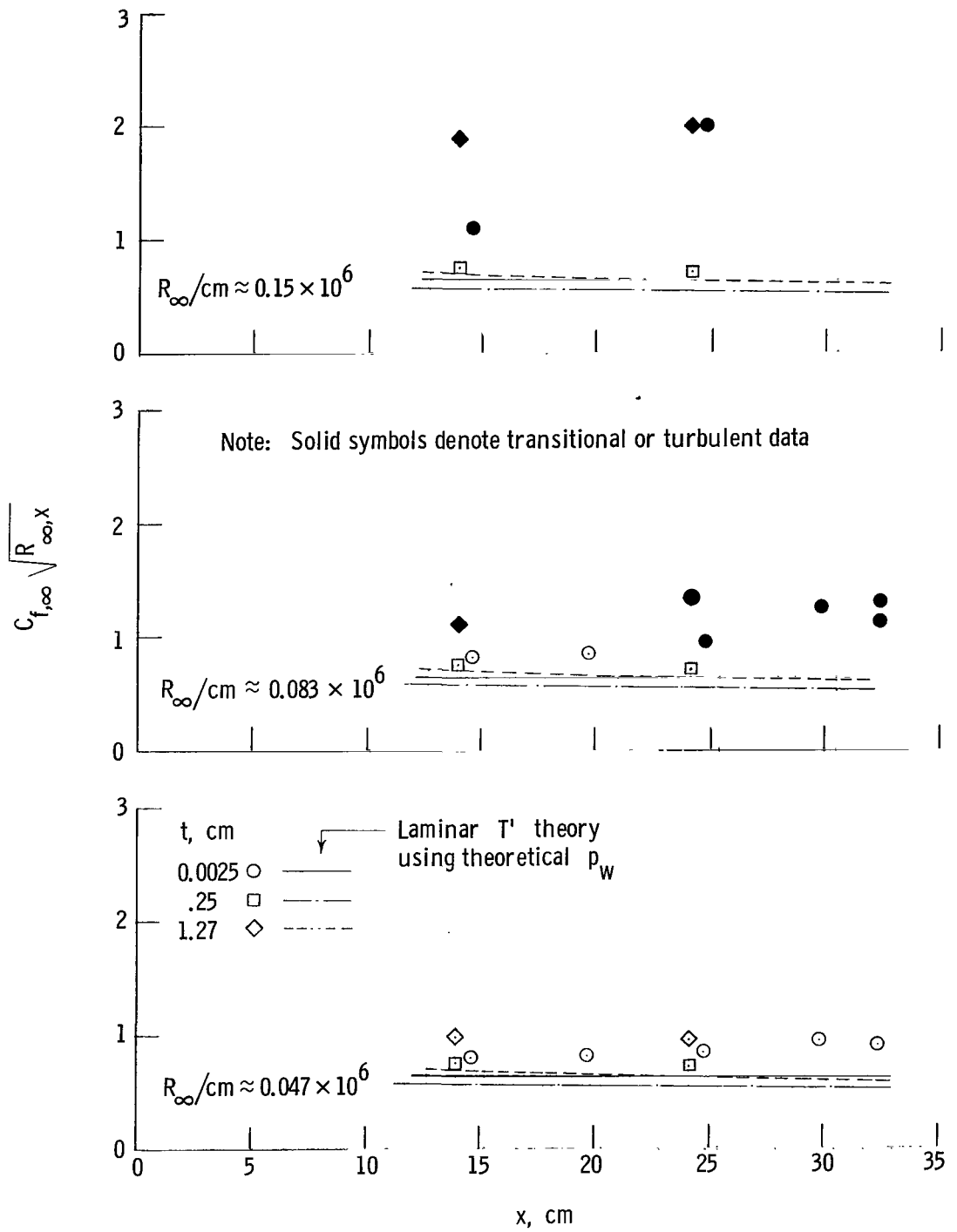
(c) $C_{f,\infty}\sqrt{R_{\infty,x}}$.

Figure 16.- Concluded.
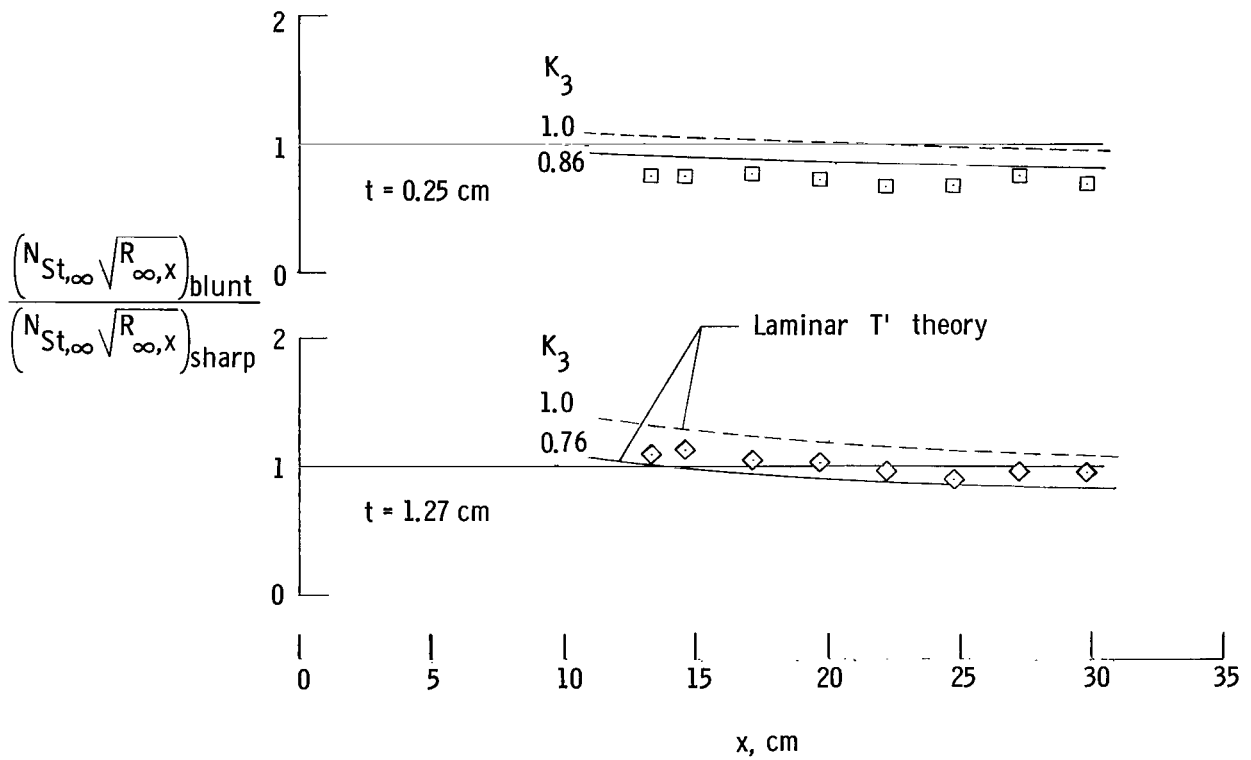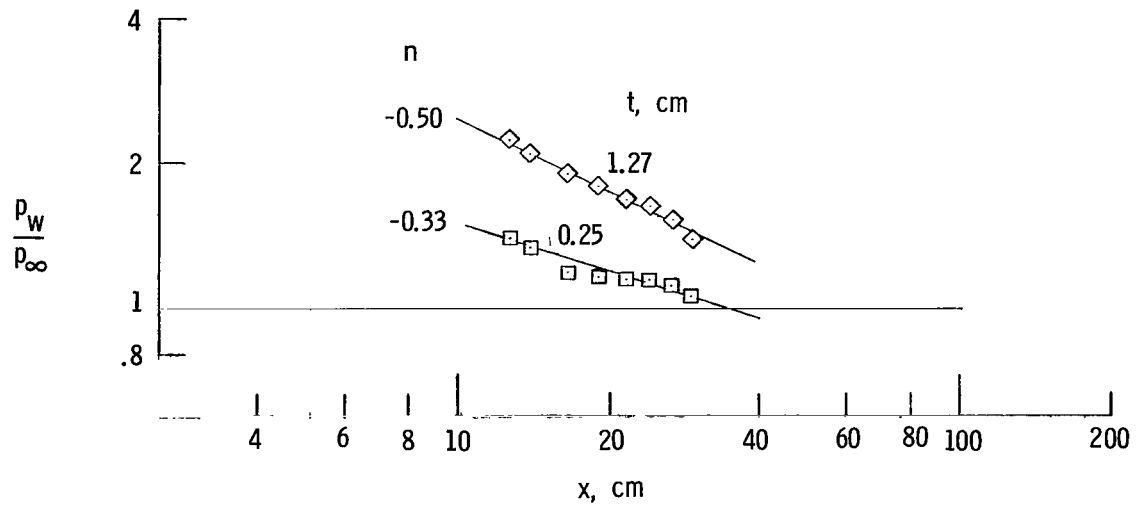
Figure 17.- Effects of pressure gradient on the laminar heat transfer. $R_\infty/cm \approx 0.047 \times 10^6$.
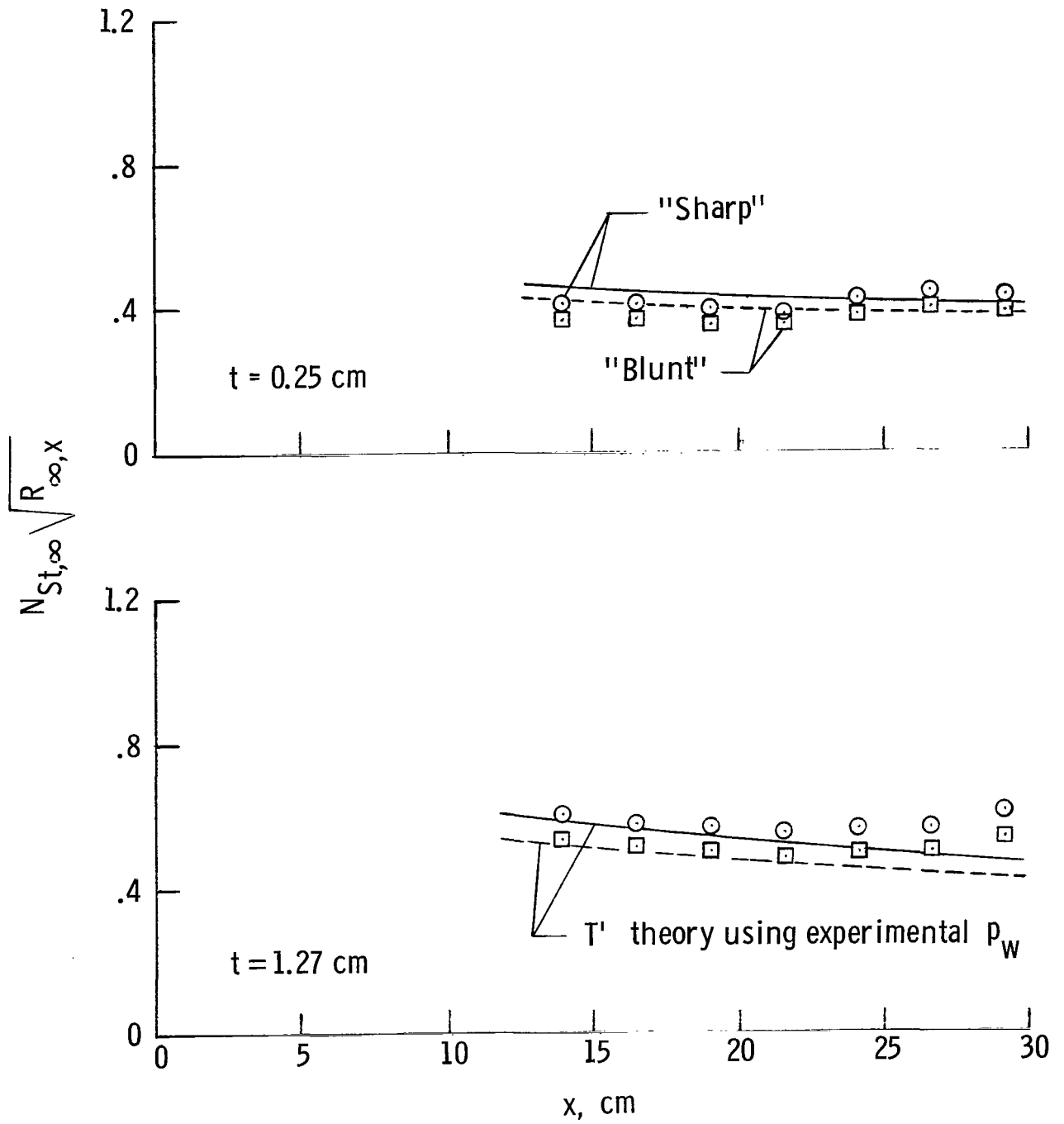
Figure 18.- Difference in value of $N_{St,\infty}\sqrt{R_{\infty,x}}$ due to normal-shock assumption ("blunt") and that due to oblique-shock assumption ("sharp").
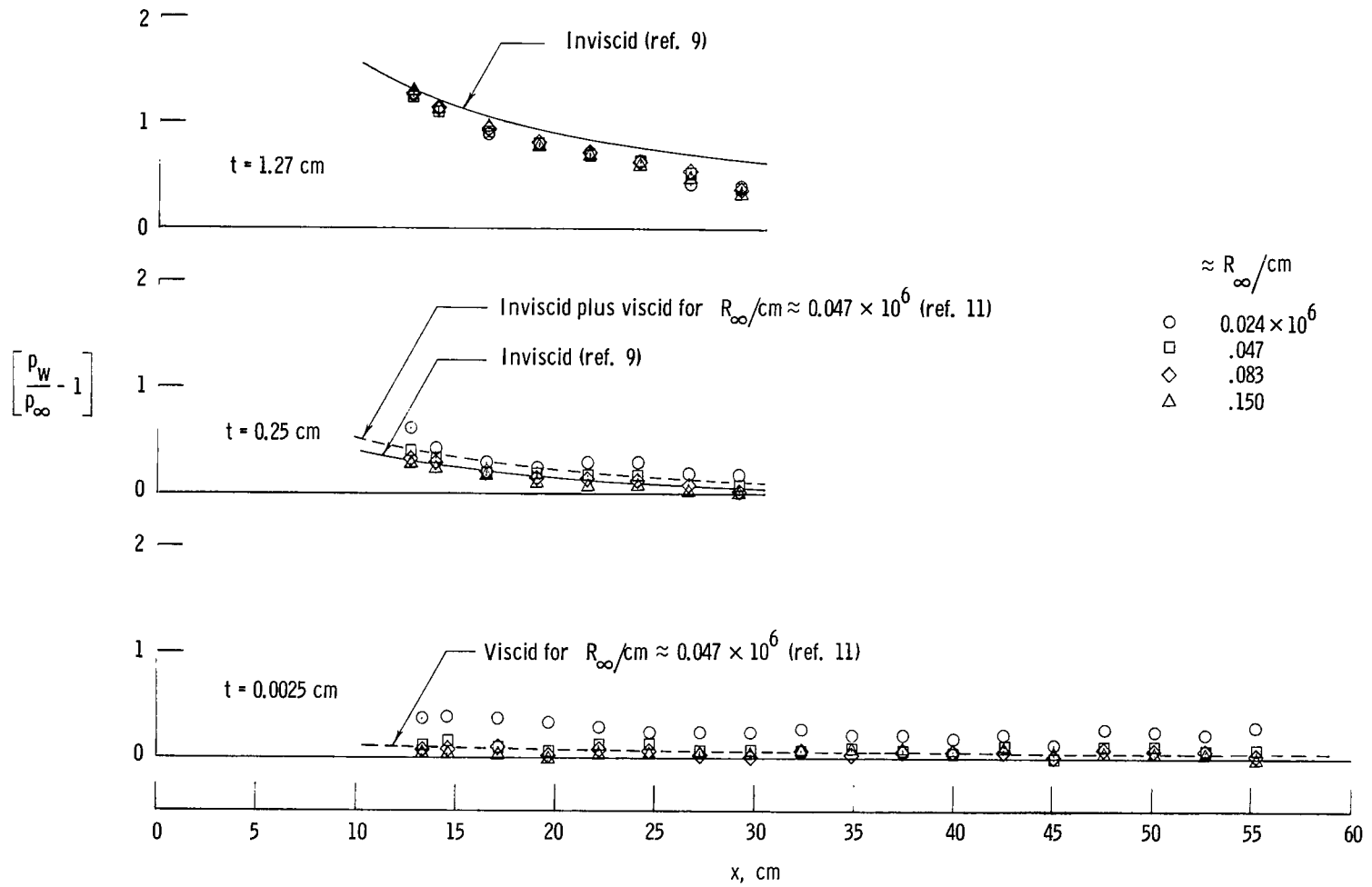
Figure 19.- Effects of Reynolds number on the induced pressure.
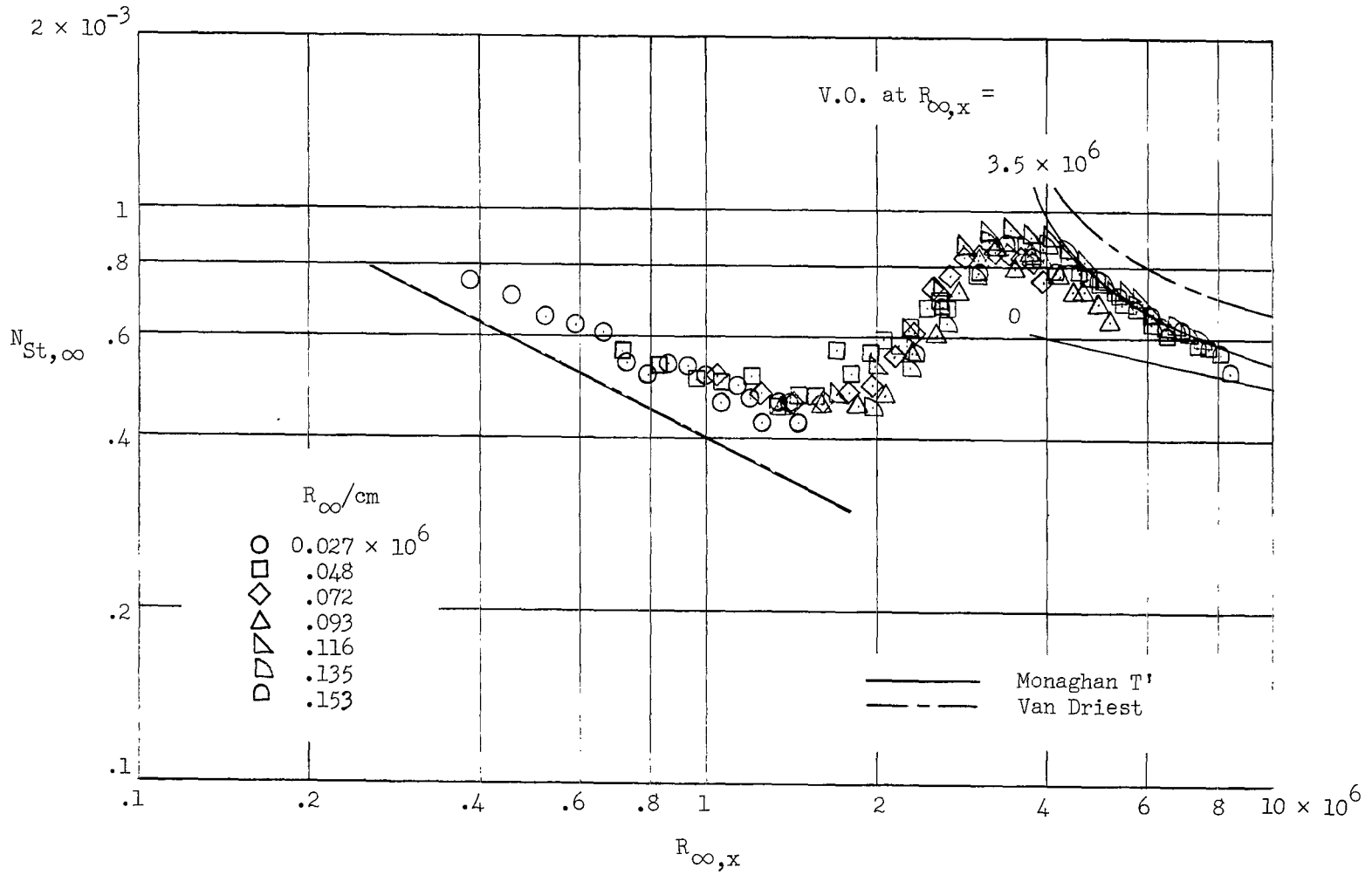
(a) t = 0.0025 cm.

Figure 20.- Variation of Stanton number with free-stream Reynolds number for various unit Reynolds numbers.
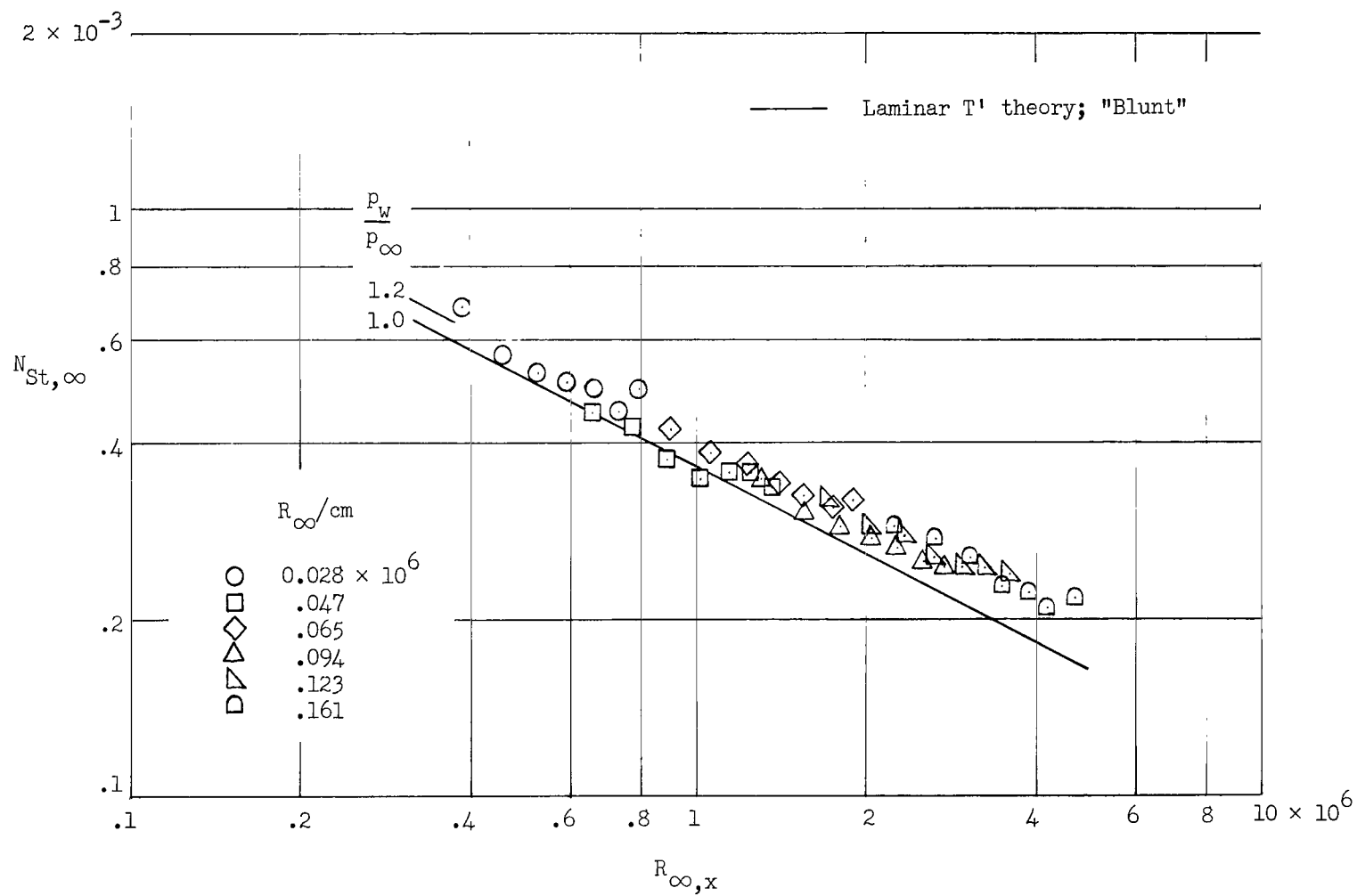
(b) t = 0.25 cm.

Figure 20.- Continued.
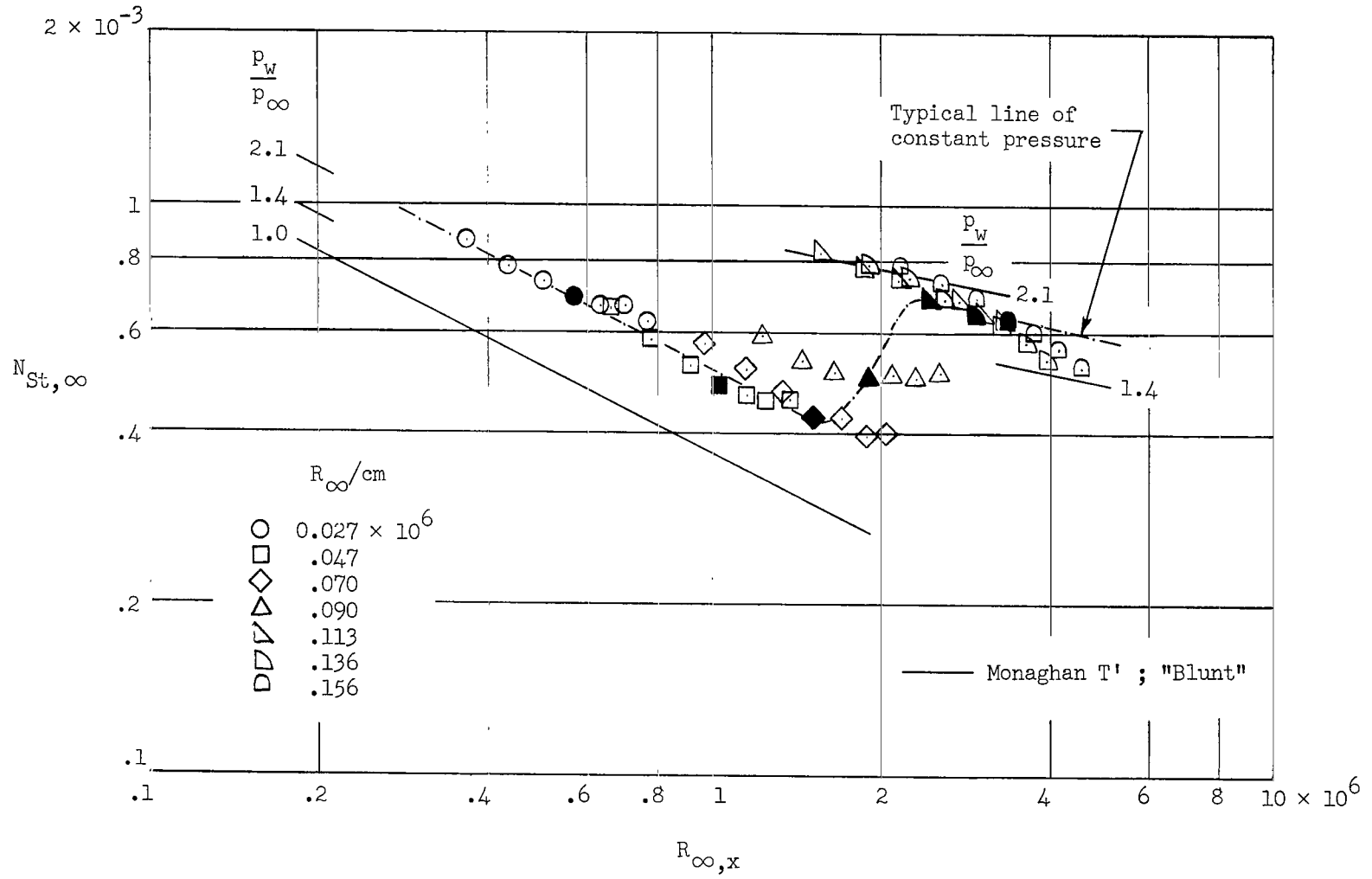
(c) t = 1.27 cm.

Figure 20.- Concluded.

1×10^{-3}

T' theory using $\left.\begin{array}{l}\text{Laminar} \\ \text{Turbulent}\end{array}\right.$
experimental p_w

$\dfrac{p_w}{p_\infty} \approx 1.4$

$\dfrac{p_w}{p_\infty} \approx 1.5$

$\dfrac{p_w}{p_\infty} \approx 1.6$

$\dfrac{p_w}{p_\infty} \approx 1.7$

$\dfrac{p_w}{p_\infty} \approx 1.8$

V. O. at:
Peak $N_{St,\infty}$

$\dfrac{p_w}{p_\infty} \approx 1.9$

Leading-edge

$\dfrac{p_w}{p_\infty} \approx 2.1$

$N_{St,\infty}$

.1   .2   .4 .6 .8 1   2   4   6 8 10×10^6

$R_{\infty,x}$
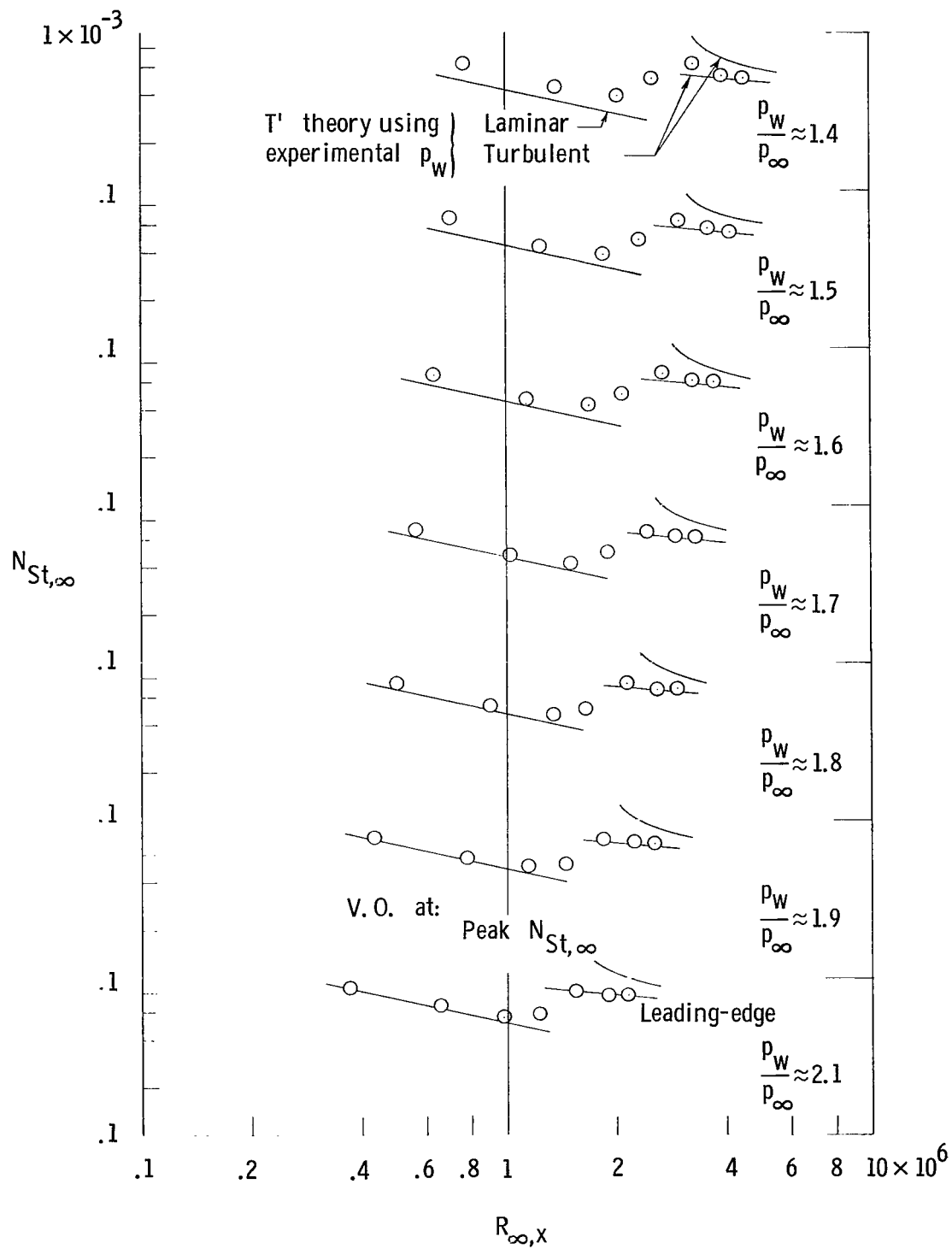
Figure 21.- Stanton number as a function of free-stream Reynolds number for the 1.27-cm-thick leading-edge model at various values of p_w/p_∞.

49
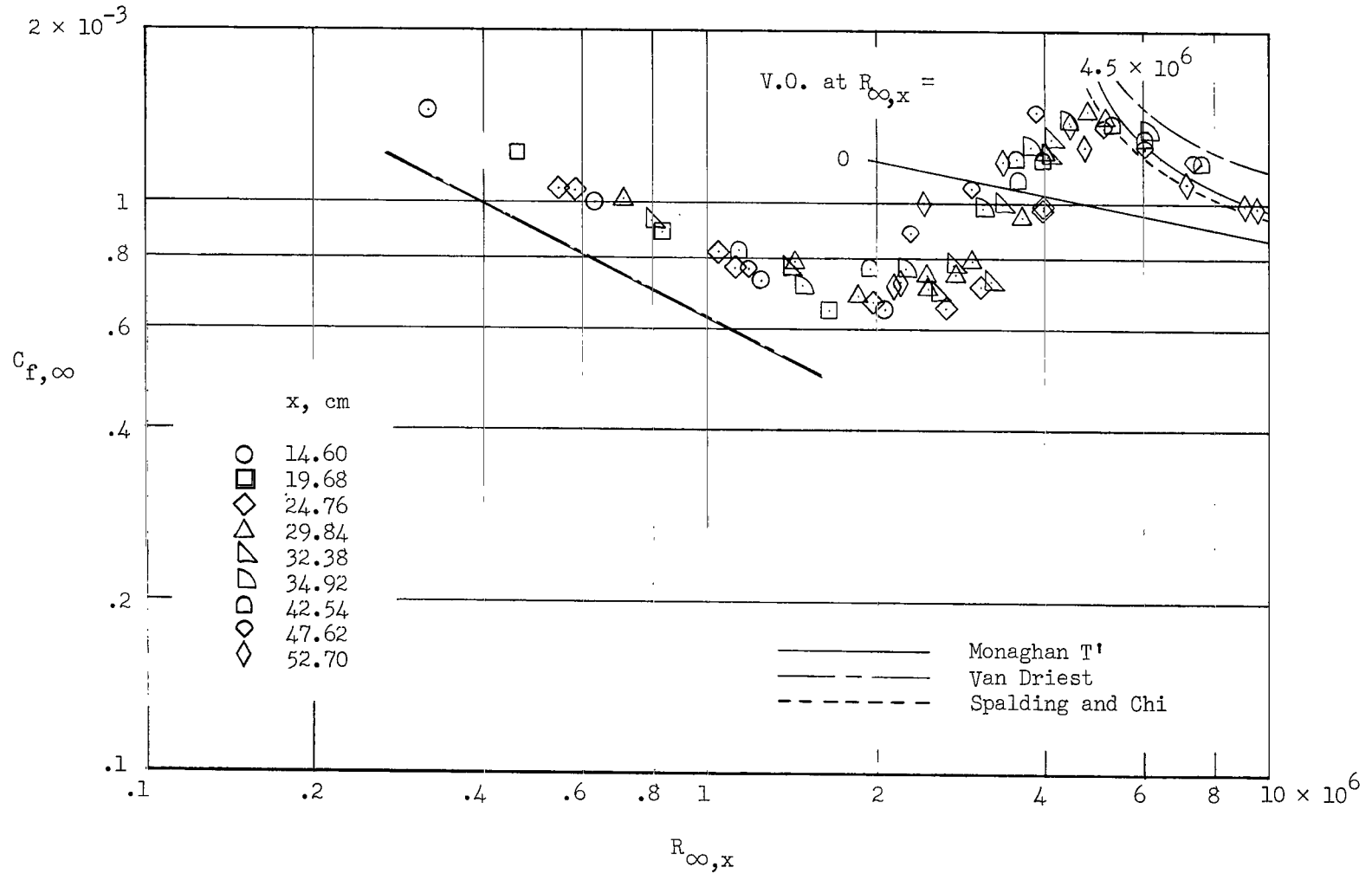
(a) t = 0.0025 cm.

Figure 22.- Variation of local skin-friction coefficient with free-stream Reynolds number for various chordwise locations.
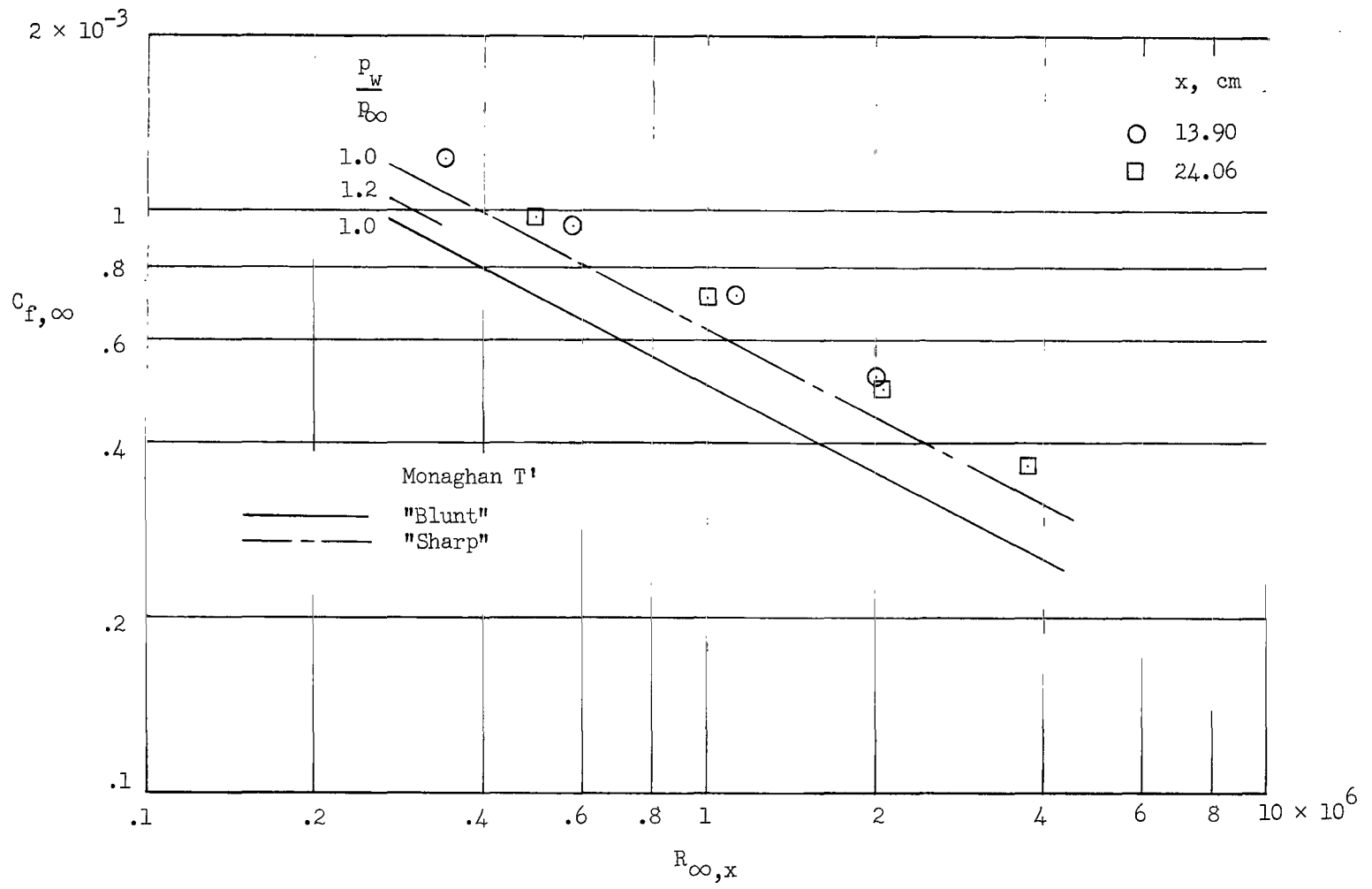
(b) t = 0.25 cm.

Figure 22.- Continued.
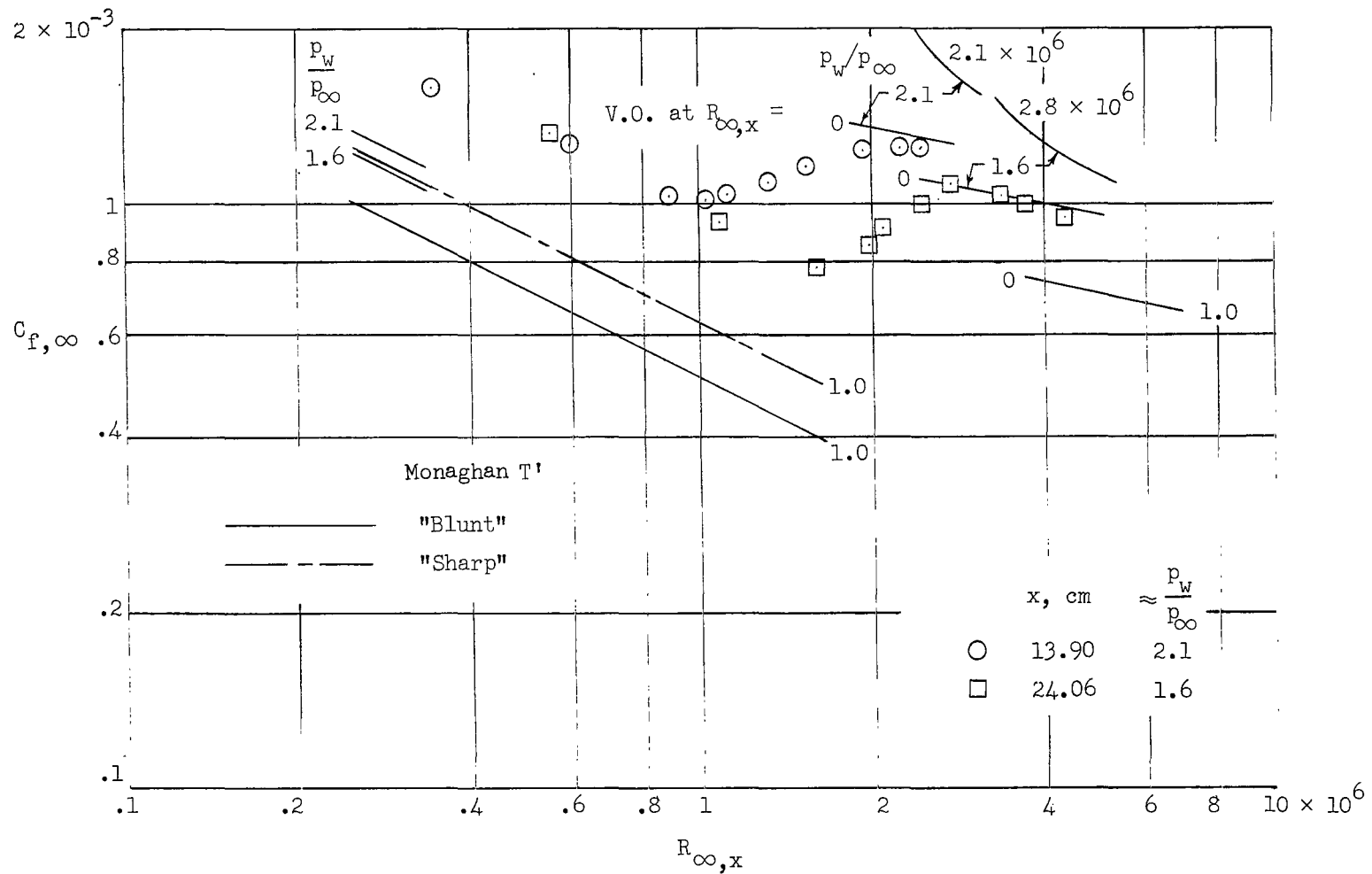
(c) t = 1.27 cm.

Figure 22.- Concluded.
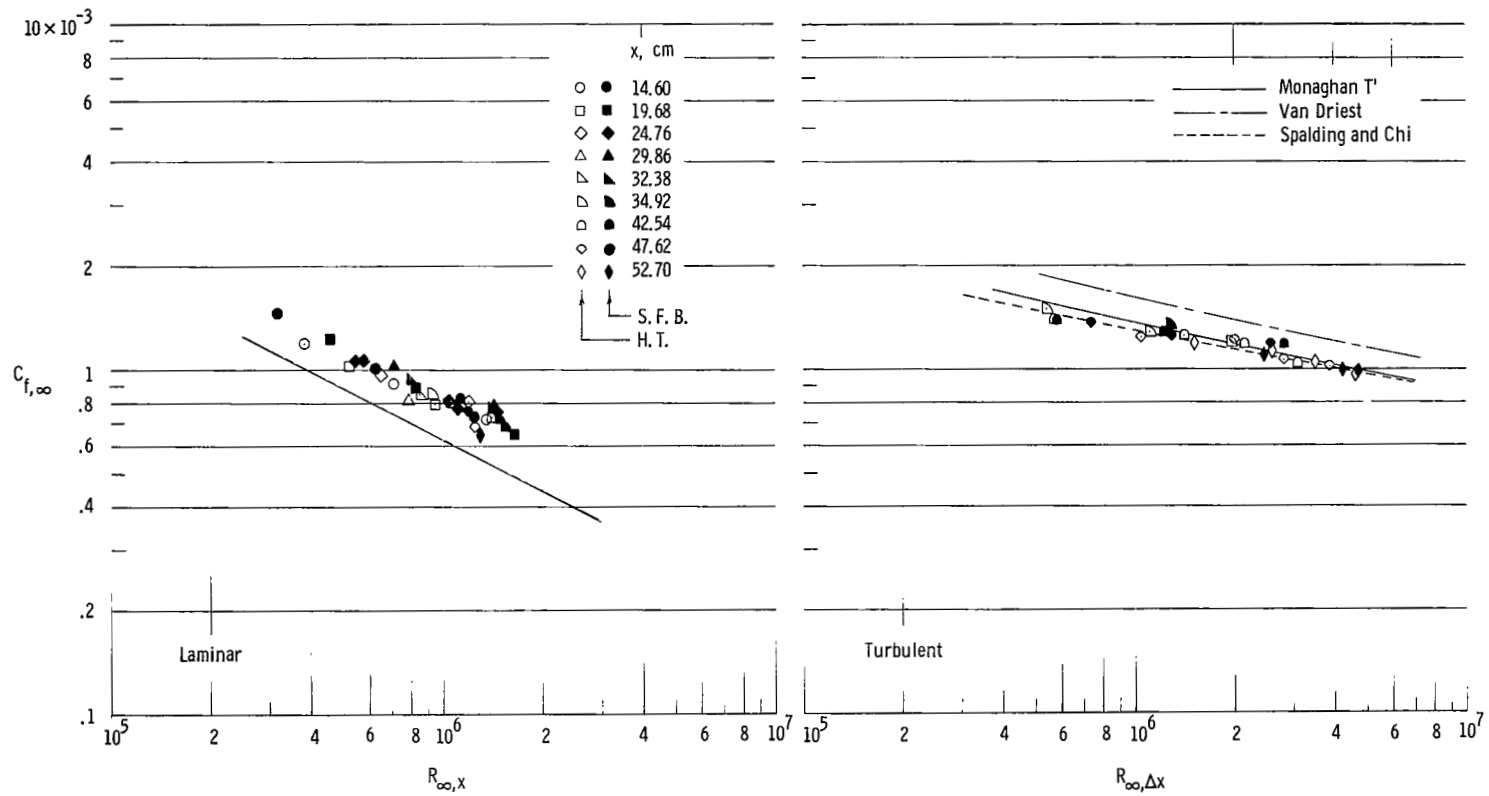
(a) t = 0.0025 cm.

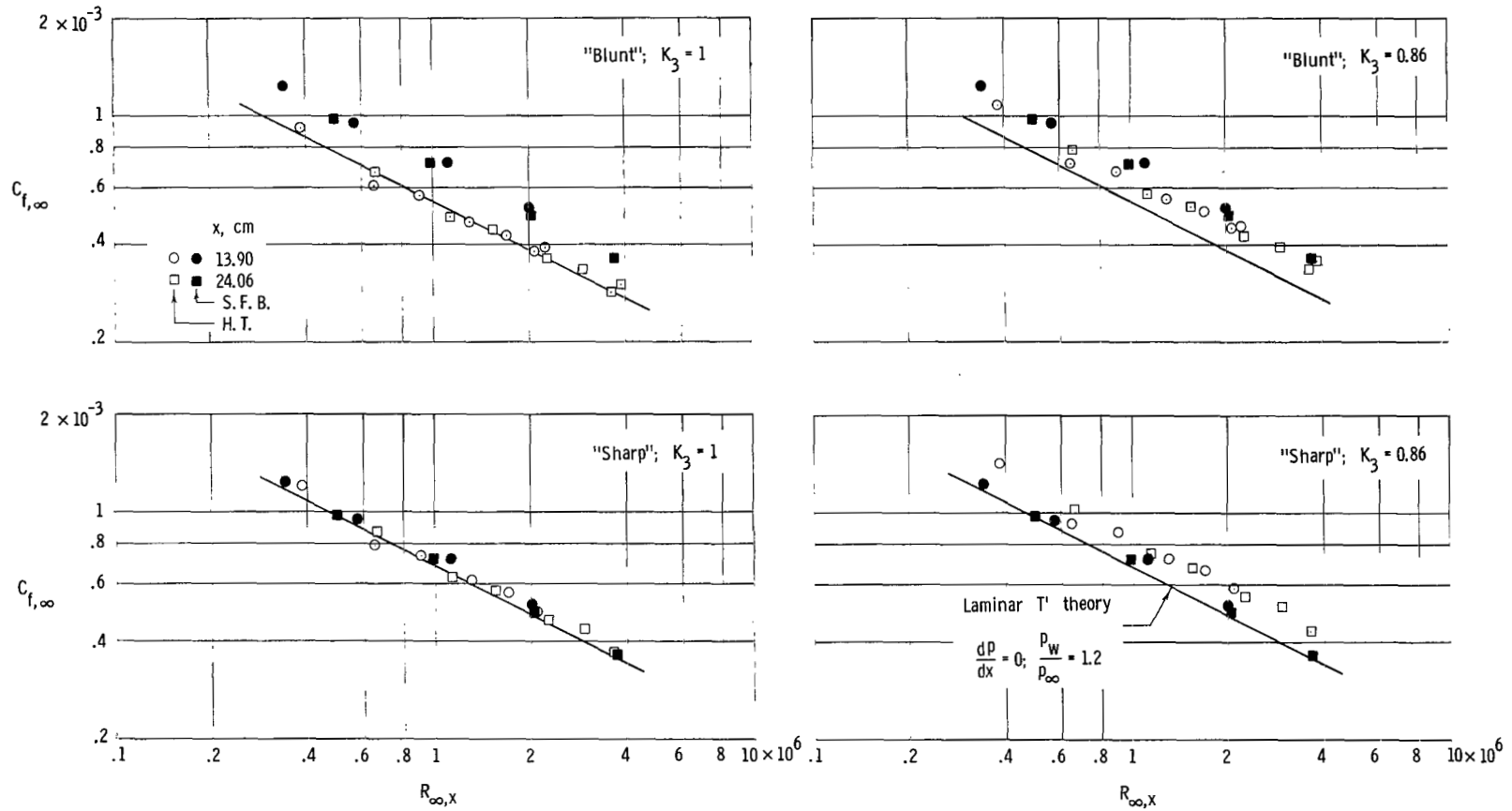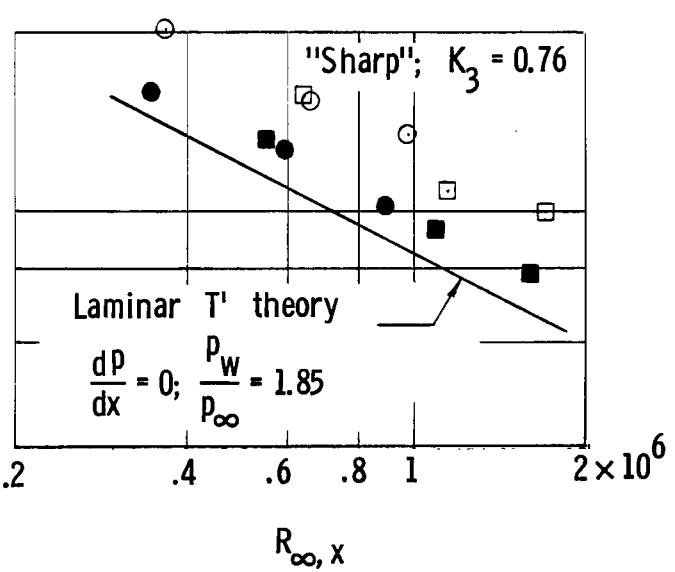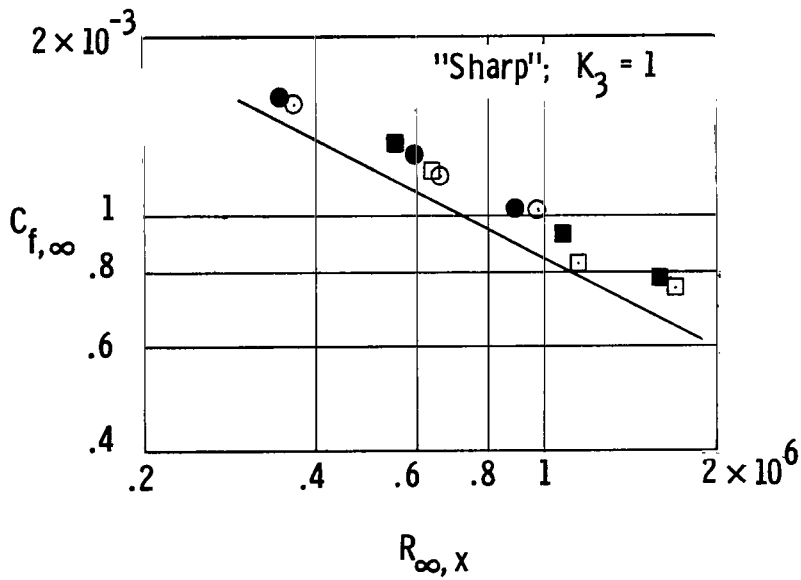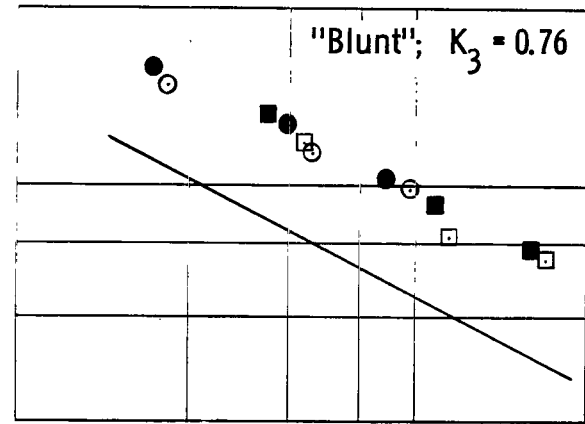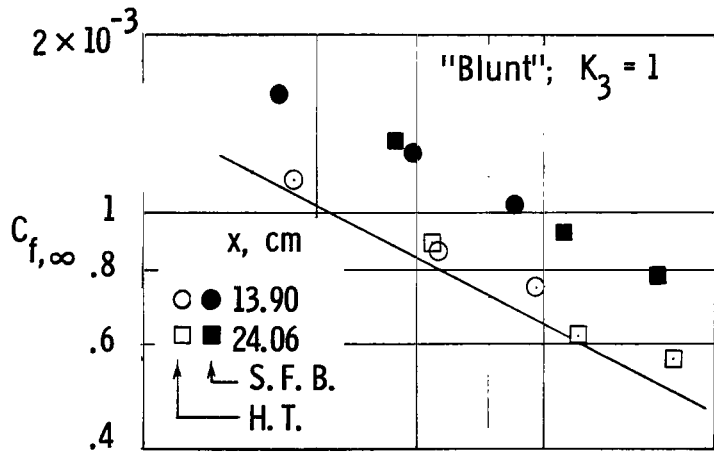Figure 23.- Comparison of the skin-friction and heat-transfer data using the Reynolds analogy concept.

(b) t = 0.25 cm.

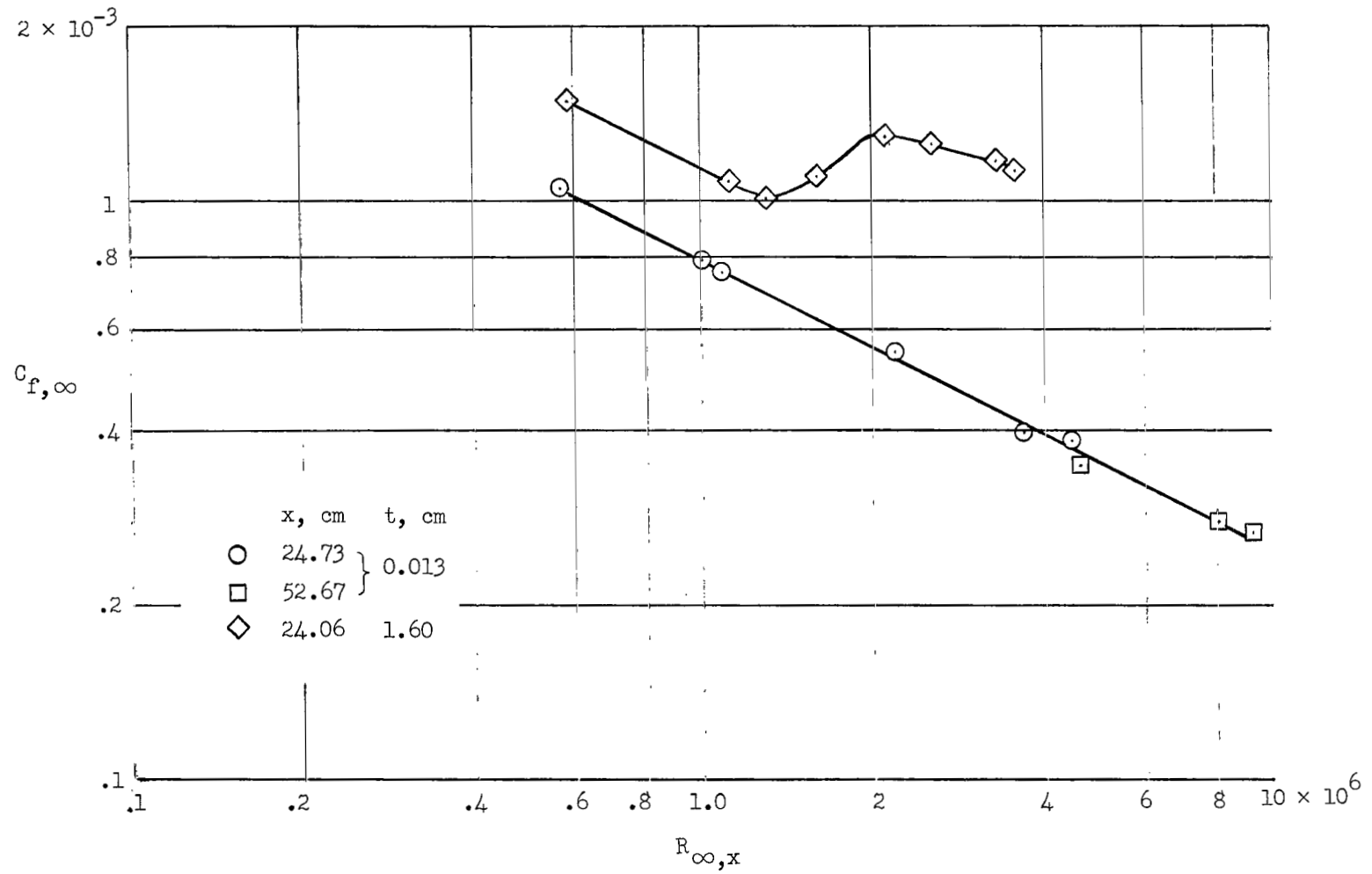Figure 23.- Continued.

(c) t = 1.27 cm.

Figure 23.- Concluded.

Figure 24.- Auxiliary skin-friction data.

"The aeronautical and space activities of the United States shall be conducted so as to contribute . . . to the expansion of human knowledge of phenomena in the atmosphere and space. The Administration shall provide for the widest practicable and appropriate dissemination of information concerning its activities and the results thereof."

—NATIONAL AERONAUTICS AND SPACE ACT OF 1958

NASA SCIENTIFIC AND TECHNICAL PUBLICATIONS

TECHNICAL REPORTS: Scientific and technical information considered important, complete, and a lasting contribution to existing knowledge.

TECHNICAL NOTES: Information less broad in scope but nevertheless of importance as a contribution to existing knowledge.

TECHNICAL MEMORANDUMS: Information receiving limited distribution because of preliminary data, security classification, or other reasons.

CONTRACTOR REPORTS: Technical information generated in connection with a NASA contract or grant and released under NASA auspices.

TECHNICAL TRANSLATIONS: Information published in a foreign language considered to merit NASA distribution in English.

TECHNICAL REPRINTS: Information derived from NASA activities and initially published in the form of journal articles.

SPECIAL PUBLICATIONS: Information derived from or of value to NASA activities but not necessarily reporting the results of individual NASA-programmed scientific efforts. Publications include conference proceedings, monographs, data compilations, handbooks, sourcebooks, and special bibliographies.

Details on the availability of these publications may be obtained from:

SCIENTIFIC AND TECHNICAL INFORMATION DIVISION

NATIONAL AERONAUTICS AND SPACE ADMINISTRATION

Washington, D.C. 20546